FEATURE ARTICLE

Elementary Steps in Excited-State Proton Transfer†

Noam Agmon*

Department of Physical Chemistry and the Fritz Haber Research Center, The Hebrew University, Jerusalem 91904, Israel

Received: June 11, 2004; In Final Form: September 25, 2004

The absorption of a photon by a hydroxy-aromatic photoacid triggers a cascade of events contributing to the overall phenomenon of intermolecular excited-state proton transfer. The fundamental steps involved were studied over the last 20 years using a combination of theoretical and experimental techniques. They are surveyed in this sequel in sequential order, from fast to slow. The excitation triggers an intramolecular charge transfer to the ring system, which is more prominent for the anionic base than the acid. The charge redistribution, in turn, triggers changes in hydrogen-bond strengths that set the stage for the proton-transfer step itself. This step is strongly influenced by the solvent, resulting in unusual dependence of the dissociation rate coefficient on water content, temperature, and isotopic substitution. The photolyzed proton can diffuse in the aqueous solution in a mechanism that involves collective changes in hydrogen-bonding. On longer times, it may recombine adiabatically with the excited base or quench it. The theory for these diffusion-influenced geminate reactions has been developed, showing nice agreement with experiment. Finally, the effect of inert salts, bases, and acids on these reactions is analyzed.

I. Introduction

Certain aromatic dye molecules undergo a dramatic change in their acidity upon electronic excitation. Photoacids (such as hydroxyaryls and aromatic amines) increase their acidity, whereas photobases (such as nitrogen heteroaromatics) increase their basicity. The effect has first been investigated by Förster and Weller,[1,2] and several reviews have since been written on this class of reactions.[3−8] When the acidic and basic moieties exist in proximity within the same molecule, one observes intramolecular excited-state (ES) proton transfer (PT).[9,10] Otherwise, the reaction is intermolecular: either bimolecular or pseudo-unimolecular, such as in the case of excited-state proton transfer (ESPT) to solvent. The long-standing interest in the photoacidity phenomenon is, from basic science perspective, because it allows the investigation of fast proton-transfer reactions and, from a practical point of view, as a means of generating protons at a specified instant of time.

* Corresponding author. E-mail: agmon@fh.huji.ac.il. Fax: 972-2-6513742.

† Abbreviations: 1OH, 1-naphthol; 1N4S, 1-hydroxynaphthalene-4-sulfonate; 2OH, 2-naphthol; 2OMe, 2-methoxynaphthol; 2N6S, 2-hydroxynaphthalene-6-sulfonate; 2N68DS, 2-hydroxynaphthalene-6,8-disulfonate; 4WM, 4 water molecule model; 5CN1, 5-cyano-1-naphthol; 5CN2 or 5CN, 5-cyano-2-naphthol; 6CN, 6-cyano-2-naphthol, etc.; 5CN2OD, deuterated 5CN; 5MS1N, 5-(methanesulfonyl)-1-naphthol; BEBO, bond energy−bond order; BO, bond order; DCN2, 5,8-dicyano-2-naphthol; DH, Debye−Hückel; DMSO, dimethyl sulfoxide; DSE, Debye−Smoluchowski equation; ES, excited state; ESPT, excited-state proton transfer; EtOH, ethanol; EVB, empirical valence bond; GS, ground state; HB, hydrogen bond; HPTS, 8-hydroxypyrene-1,3,6-trisulfonate; ICT, intramolecular charge transfer; IR, infrared; IRF, instrument response function; ISM, intersecting-state model; KIE, kinetic isotope effect; MPK1, multi-particle kernel 1; MS-EVB, multi-state empirical valence bond; R2PI, resonance 2-photon ionization; S, solvent molecule; SSDP, spherical symmetric diffusion problem; TCSPC, time-correlated single photon counting; TEBO, total effective bond order; TS, transition state; USA, unified Smoluchowski approximation.

SCHEME 1: Structure of 2OH with the Atom Numbering Used in This Sequel

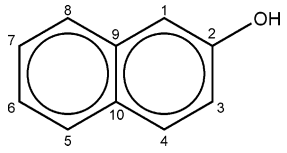

SCHEME 2: Cycle of 2OH Excitation and Photodissociation[3]

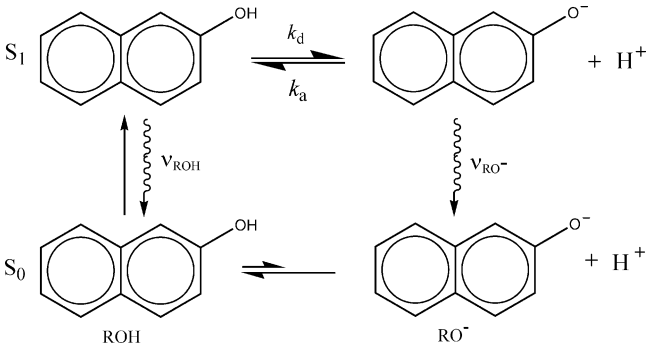

For concreteness, we focus in this review on hydroxyaryls (ROH, where R is an aromatic ring system) such as 2-naphthol (2OH, Scheme 1) and its derivatives. The pK_a value of 2OH drops from 9.5 in the ground, S_0, electronic state to 2.8 in its first excited singlet state, S_1. (We often designate the ES by an asterisk and its pK_a value by pK_a^*). The full cycle that it undergoes following photon absorption is known as the "Förster cycle" and is depicted in Scheme 2. In the ground state (GS), the acid form dominates, and it is converted to an excited 2OH

10.1021/jp047465m CCC: $30.25
Published on Web 12/17/2004

SCHEME 3: Structure of Four 2OH Cyano Derivatives with Their Ground[12,13] and the Diffusion Model Excited-State[14] Acidity Constants (Boxed, Upper and Lower Values, Respectively)

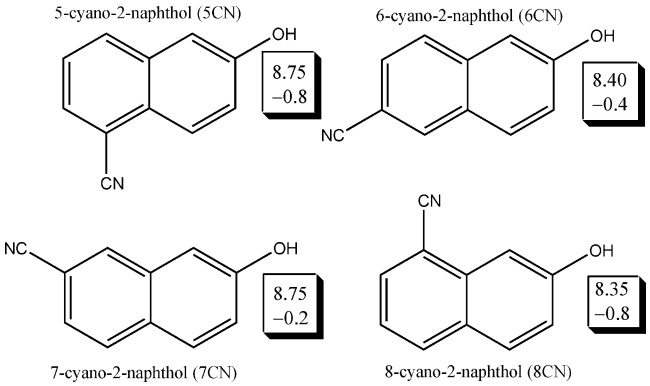

molecule by photoexcitation. The latter undergoes a reaction of ESPT to solvent

$$\begin{array}{ccc} \mathrm{R^*OH} & \underset{k_a}{\overset{k_d}{\rightleftharpoons}} & \mathrm{R^*O^-} + \mathrm{H^+} \\ \downarrow k_0 & & \downarrow k_0' \end{array} \qquad (1.1)$$

Its dissociation rate constant is k_d, where $1/k_d$ is typically in the range of 1−1000 ps. The dissociation process generates the (R^*O^-/H^+) ion pair at their "contact" distance, a, from which they may associate with the rate constant k_a. The separation of the partners over a distance r requires overcoming an attractive electrostatic potential $V(r)$ (in units of the thermal energy, k_BT). Thus, the overall acid constant (equilibrium dissociation constant) is $K_a^* = k_d \exp[V(a)]/k_a$, and $pK_a^* \equiv -\log K_a^*$.

Both excited species, R*OH and R^*O^-, decay to their ground state in a few (typically, 1−10) nanoseconds, by a combination of radiative and nonradiative processes (rate constants k_0 and k_0', respectively). The light emitted (termed "fluorescence" because of the singlet level involved), occurs at different wavelengths for the acid and base. Because dissociation is more downhill in S_1, the $S_1 \rightarrow S_0$ gap is smaller for the anion, so that the R^*O^- fluorescence is red shifted as compared with that of the R*OH. For example, the peak fluorescence frequencies of 2OH are 350 and 420 nm for the acid and base forms, respectively.[11] These two frequencies, together with the GS pK_a, could allow one to calculate pK_a^* via this Förster cycle. Such a determination may be inaccurate, because the solvent relaxes around the R*OH after excitation, and around the R^*O^- after proton dissociation. Some aspects of these relaxation processes are discussed below, as well as a more accurate diffusion model for determining the two rate coefficients and hence the pK_a^* value.

To probe the reaction over a wider range of photoacidities, it is useful to consider a whole class of 2OH derivatives. Scheme 3 shows the structure of four cyano-substituted 2OH molecules, synthesized by Tolbert and collaborators.[12] The pK_a and pK_a^* values are indicated near each structure.[13,14] It is evident that the "electron-withdrawing" CN group makes these molecules more acidic than 2OH: Slightly so in S_0, and more dramatically so in S_1. These dye molecules can thus transfer their proton not only to water but also to various alcohols. The doubly substituted CN derivatives (not shown) are almost as strong as a mineral acid [e.g., $pK_a^* = -4.5$ for 5,8-dicyano-2-naphthol (DCN2)]. They can undergo proton transfer to various organic solvents, such as dimethyl sulfoxide (DMSO). Thus the investigation of ESPT can be extended to a variety of solvents besides water.[15−18]

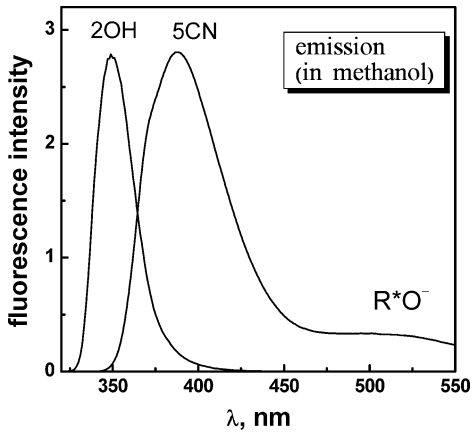

Figure 1. Steady-state fluorescence spectrum of 2OH and its 5-cyano derivative in pure methanol. Adapted from Figure 4 of ref 17.

As an example, Figure 1 compares the steady-state fluorescence spectrum of 2OH and 5-cyano-2-naphthol (5CN) in methanol. 2OH does not transfer its proton to pure methanol, and therefore only its ROH band (350 nm) appears. For 5CN, ESPT to methanol does occur. Therefore, in addition to its ROH band (388 nm) a strongly red-shifted RO^- band appears (around 510 nm). In addition, the ROH band is also red shifted with respect to that of 2OH, which shows that the cyano substituent stabilizes both forms of the excited 2OH, a phenomenon that will be discussed below.

During the course of an ESPT reaction (Scheme 2), one may envision numerous consecutive elementary processes occurring over some 8 decades in time, from subfemtosecond to submicrosecond time scales. The present report is possibly the first unified exposition of this sequel, from the fastest to slowest time scales. Though most of the observations below could be quite general, some might nevertheless be restricted to naphthol and similar hydroxy-aromatic derivatives.

The fundamental processes to be discussed include electronic redistribution upon excitation (subfemtosecond), hydrogen-bond (HB) rearrangements near the OH group (femtosecond), proton dissociation followed by proton solvation and mobility (picosecond), geminate recombination of the dissociated proton with the conjugate photobase, quenching and ES decay (nanosecond). These slower processes are distinctly diffusion-influenced;[19] hence their study also sheds light on the features of such reactions in solution. These reactions are further complicated in the presence of salts, bases, or acids. The main theoretical tools required for treating these reactions are presented, together with their corresponding experimental verification. At the end, a few applications of ESPT are mentioned, but their comprehensive discussion requires a separate review article.

II. Electronic Redistribution

The first event that occurs upon excitation is redistribution of the π electron cloud, producing the electron-density characteristic of the excited S_1 state. Weller[20] first proposed that this involves intramolecular charge transfer (ICT) from the oxygen atom to the aromatic ring system. The reduced electron density on the hydroxyl group weakens the OH bond, making proton dissociation more facile, whereas the excess electron density migrates in naphthols to the distal ring (namely, the one not attached to the OH group).[5,21−25]

This description is somewhat misleading, because it creates the impression that the origin of the enhanced photoacidity is

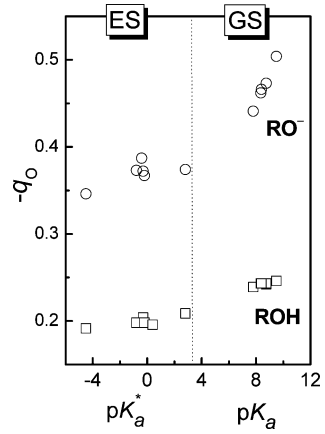

Figure 2. Correlation of the calculated[29] gas-phase Mulliken charge on the oxygen atom of 2OH and its cyano derivatives (5CN, 6CN, 7CN, 8CN and DCN2) with their experimental acidity constants in solution (see Scheme 3). Adapted from Figure 3 of ref 29.

in the acid form.[26] However, if ICT occurs spontaneously, it should stabilize the R*OH, and this would make its dissociation more uphill. Therefore, the increase in k_d must arise from an even larger ICT effect on the R*O$^-$ anion, where a full formal charge needs to be delocalized.[20,23,27] This has been verified by ab initio calculations on phenol and *p*-cyanophenol, whose dipole moments show a significant decrease in absolute value upon excitation only for the anionic base.[26]

Naphthols and their derivatives (as well as ortho- and meta-substituted phenol) have a lower symmetry than phenol, and therefore the variation in dipole moment is not a good monitor for the charge distribution. In these cases one could still learn about the ICT effect by probing the molecular charge distribution directly. Using the AMPAC 6.55 package,[28] we have performed extensive semiempirical AM1 calculations on gas-phase 2OH and its cyano derivatives, for both acid and basic forms in their first 3 singlet states.[29] (The study includes the mono-cyano derivatives and DCN2). Let us consider the observed effects on the oxygen end and the aromatic rings.

A. Effects at the Oxygen End. From the ICT ansatz, one may expect a decrease in the electronic charge density on the oxygen atom upon excitation, which should be larger for the anion than for the acid and should further increase for more acidic photoacids. The results in Figure 2 verify this expectation.[29] It correlates the Mulliken charges on the oxygen atom (q_O) with the corresponding experimental solution-phase pK_a and pK_a^* values. For each of the six molecules studied, four data points are included in the figure: for S_0 and S_1 (right and left of the dashed line, respectively) and the acid and base forms (squares and circles, respectively). For ROH the charge is small and varies only slightly with the pK_a. For RO$^-$ the charge is large and varies more conspicuously, particularly when the transition from S_0 to S_1 is considered. The calculation thus directly verifies the operation of the ICT effect, which is small for the acid and large for the base.

Additional support for the ICT effect is obtained from the calculated C−O bond lengths.[29] In GS 2OH, it is around 1.37 Å for the acid, shortening to 1.26 Å in the anion. Thus the GS anion is stabilized by a quinoid resonance structure (Scheme 4), with the negative charge distributed on the indicated ring sites. Electron-withdrawing cyano substituents further shorten this bond. Figure 3 shows a remarkable correlation between the calculated C−O bond lengths in the RO$^-$ derivatives and the GS pK_a values. Two distinct correlation lines are observed: The upper one for S_0 and the lower one (more scattered) for S_1.

SCHEME 4: Five Possible Quinoid Resonance Structures of 2-Naphtholate in Its GS

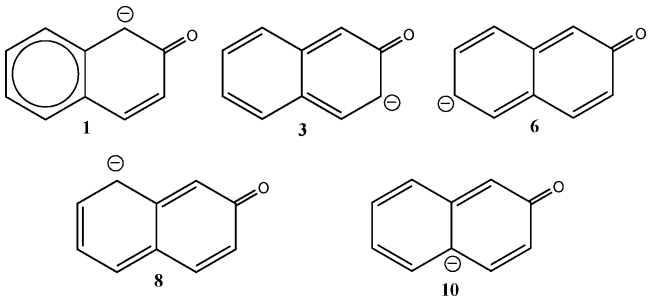

Thus excitation further shortens the C−O bond, indicating an enhanced double-bond character with increasing ICT effect.

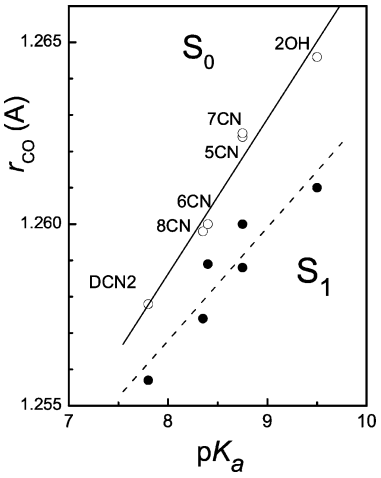

Figure 3. Correlation of the calculated[29] C−O bond lengths in gas-phase RO$^-$ (circles), with the GS solution-phase acidity constant of 2OH and its cyano derivatives. Full line correlates the bond lengths in S_0 whereas the dashed line is for S_1. Adapted from Figure 4 in ref 29.

B. Effect on the Aromatic Rings. The charge density that migrates from the oxygen does not disperse uniformly on the aromatic rings but is rather directed toward specific sites. Figure 4 shows a color-coded electron-density map of the acid and base forms of 2OH in their first two singlet states, as deduced from the AM1 calculations.[29] As usual, red represents the most positive atoms, yellow is neutral, and blue is the most negative.

For ROH, the ring charges are relatively uniform, except at the sites immediately adjacent to the OH group. There is some excess electronic charge in position 1 and some deficiency in position 2. Upon excitation, the charge from the oxygen moves predominantly to position 3. In particular, there is no electron-density transfer to the distal ring (the total charge in positions 5−10 remains constant). Although this contrasts with the conventional view of the ICT effect, it may be due to the lack of solvent in these calculations (see discussion in section IIIC below).

The situation is different for the RO$^-$ with its formal −1 charge. Already in the GS some of this charge finds its way to the aromatic ring sites. As compared with GS ROH, the sites that gain most of the electron density are 1, 3, 6, 8, and 10 (whereas carbon 2 becomes more positive). These electron-enriched positions coincide with the location of the excess charge in the five possible resonance structures of 2-naphtholate (Scheme 4). The valence-bond picture is thus quite useful for the GS.

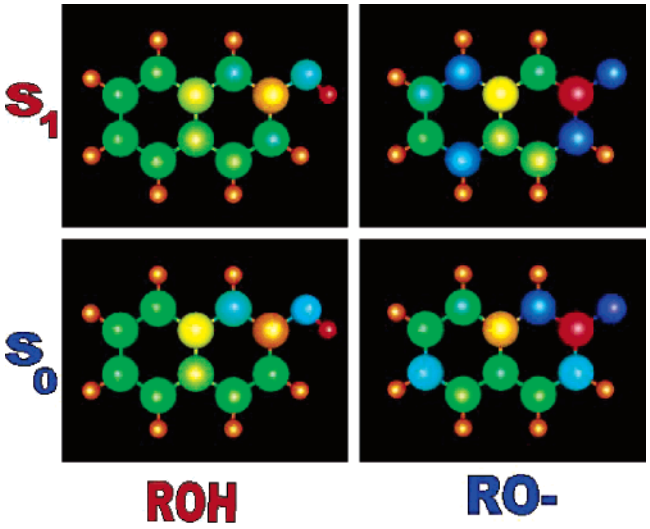

Figure 4. Electron density on 2-naphthol (ROH) and 2-naphtholate (RO^-) in their first two singlet states. From Tables 3 and 5 of ref 29. Color code: red, most positive; orange, slightly positive; yellow, neutral; green, slightly negative; blue, most negative.

Upon excitation to S_1, we find pronounced changes in the ring charge densities. In the proximal ring, the electronic charge diminishes in position 1 and increases in position 3. This is similar to the behavior observed for ROH, only larger. Unlike the case of ROH, there is now charge migration to the distal ring, predominantly to sites 5 and 8 (whereas the charge density on position 6 diminishes). Though this agrees with the conjecture of ICT to the *distal* ring, the valence-bond structures in Scheme 4 are not useful in explaining it (in particular, there is no resonance structure with negative charge at C5).

C. Experimental pK_a Values. The electronic distributions discussed above explain the large enhancement of photoacidity by electron-withdrawing cyano substituents on the distal ring. Because ICT to the distal ring occurs only for the anion, but not for the acid (where charge migrates to the proximal ring), these distal substituents are expected to stabilize exclusively the anionic base. The ES reaction thus becomes more downhill, resulting in enhanced photoacidity.

The cyano substituents are sensitive not only to the average charge of the distal ring, but even to the site to site charge modulations. Thus the charge variations in positions 5−8 of the 2OH anion (Figure 4) may explain the experimental pK_a values for the corresponding cyano derivatives, as summarized in Scheme 3. In the GS of RO^-, positions 6 and 8 are the most electronegative, in agreement with the corresponding resonance structures in Scheme 4. Consequently, the pK_a values of 6CN and 8CN are lower, by 0.4 pK units, than those of 5CN and 7CN. This difference is larger than the error bars for GS pK_a determination.

For the ES, the pK_a^* values depend on their method of determination. We believe that the diffusion model analysis of time-resolved data (section VIA) gives more reliable results than the traditional Förster cycle or fluorimetric titration methods.[2−4] Therefore the diffusion model pK_a^*'s are given in Scheme 3. According to these data, 5CN and 8CN are more acidic (by about 0.5 pK units) than 6CN and 7CN in their S_1 state. This agrees with the calculation which shows that positions 5 and 8 become the most electronegative in the distal ring (Figure 4). The agreement holds although the calculation is for gas-phase molecules, whereas the experimental data are for water.

SCHEME 5: Carbon−Carbon Bond Lenths in 2-Naphtholate S_0 (Upper Entries) and S_1 (Lower Entries) States (from Table 8 of Ref 29)

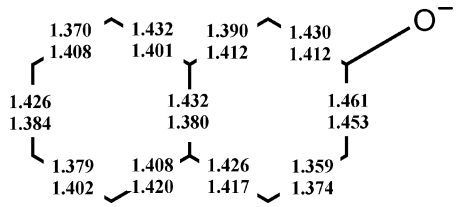

D. Photoacidity and Aromaticity. The classical explanation of photoacidity via the ICT effect leaves several open questions:

(a) Why is ES−ICT from the oxygen center larger for the anion than the ROH form?

(b) Why is the charge in the distal ring enhanced *only* by exciting the anion?

(c) Why is photoacidity observed only for aromatic dyes?

To understand these issues, it is useful to consider some basic notions in the study of aromaticity.[30] Small aromatic molecules often conform to Hückel's $4n + 2$ rule.[31] Benzene is an aromatic molecule ($n = 1$) whereas cyclobutadiene, with its $4n$ π electrons ($n = 1$), is anti-aromatic. As a result, its GS structure is distorted from square-planar to a rectangle, with two short ("double") bonds and two long ("single") bonds. Although it is known that it becomes aromatic in its first triplet state (T_1), only recently was it pointed out that cyclobutadiene is a perfectly square aromatic molecule also in its S_1 state.[32] Thus the aromatic/anti-aromatic character of a small ring system inverts between S_0 and S_1.

For 2-naphtholate, any attempt to delocalize a pair of oxygen electrons on the aromatic rings creates a $4n$ π electron system ($n = 3$), which should possess some anti-aromatic character in the GS. As a result, the structure should distort, leading to alternating short/long C−C bonds around the ring. This was verified by the AM1 calculations,[29] which show larger bond alternation for the GS anion (Scheme 5) than for the acid. In the ES, we expect the anion to become more aromatic, and this is indeed manifested by diminishing C−C bond-length alternation (Scheme 5). The reduction in the anti-aromatic character allows the distal ring of R^*O^- to accept some of the electron density from the oxygen, with a net effect of stabilizing the excited anion.

III. Spectral Shifts: Solvent and Substituent Effects

Changes in electron density may be probed by spectral shifts in either the absorption or the emission spectra. In addition, a comparison of the two spectra (e.g., their Stokes shift) reveals information on nuclear rearrangements that follow the electronic excitation. Fortunately, 2OH and its derivatives have a simple molecular structure that allows us to separate the effect on the hydroxyl moiety from that on the aromatic rings. This facilitates the comparison with the quantum chemistry results of the previous section. By monitoring solvent-induced spectral shifts ("solvatochromic shifs"), we obtain important information concerning the HBs between solvent molecules and the oxygen center, for both acid and base forms. These HBs are seen to respond to modifications in the oxygen charge. Using specific chemical substitutions on the distal aromatic ring, we probe the site-specific electron density predicted by the quantum calculations.

A. Differential Solvatochromism Reveals Specific ROH Solvation. The solvation of the ROH molecule may involve

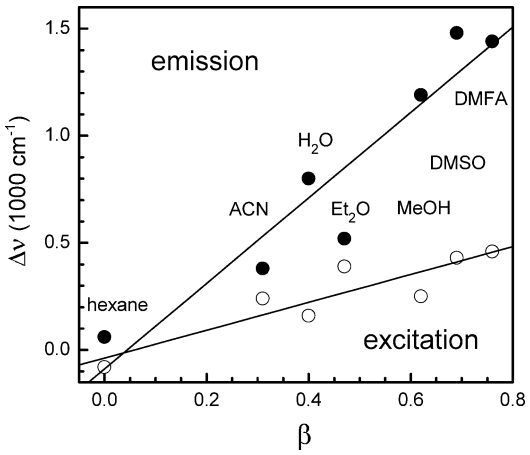

Figure 5. Differential solvatochromism of 5CN relative to its methoxy derivative in various pure solvents for excitation[36] (open circles) and emission (full circles). $\Delta\nu$ is from eq 3.1, and β is the Kamlet−Taft measure of HB acceptance by the solvent.[34] Solvent abbreviation: ACN = acetonitrile, Et_2O = diethyl ether, MeOH = methanol, DMSO = dimethyl sulfoxide, DMFA = dimethyl formamide. Data from Table 1 of ref 16.

nonspecific dipolar solvation[33] and specific solvation, particularly HBs to the hydroxyl group. There might be two such bonds. The first is a ROH···**S** bond formed with a HB accepting solvent molecule, **S**. The second is a RHO···H**S** bond formed with a protic solvent, H**S**. We have used solvatochromic shifts[15,16,27] with a Kamlet−Taft analysis[34,35] to reveal the major role played in ROH solvation by the ROH···**S** bond.

For this end, we compared the solvatochromic shifts for 2OH with its methoxy derivative, 2OMe,[27] and similarly for 5CN.[15,16] Replacement of the hydroxyl hydrogen by a methyl group eliminates the ROH···**S** bond, whereas the dipolar effects on ROH and ROMe are thought to be similar. Consequently, by subtracting the peak frequencies for the two species

$$\Delta\nu = \nu(\mathrm{ROMe}) - \nu(\mathrm{ROH}) \qquad (3.1)$$

one expects to retain only the effect of the ROH···**S** bond. We call this approach "differential solvatochromism".

Figure 5 shows a correlation of $\Delta\nu$ for 5CN with the empirical Kamlet−Taft parameter β, which depicts the solvent HB accepting power.[34,35] The nice correlation indicates that the effect of the nonspecific dipolar solvation has indeed been largely eliminated. The observed red shift ($\Delta\nu > 0$) of the hydroxy vs the methoxy compound is commensurate with the ICT ansatz. Because during the electronic transition there is no time for nuclear rearrangement, the HB must have been there already in the GS, and it serves as a probe for the electronic-density change on the OH group. The hydroxyl group becomes more positive upon excitation (Figure 2), producing a stronger ROH···**S** bond. This HB thus stabilizes the ES more than the GS, leading to the red shift. The stronger the H-bonding propensity of the solvent (as depicted by its larger β value), the larger the relative stabilization of the R*OH and hence the larger $\Delta\nu$ becomes. A similar behavior is observed for 2OH, but there the shifts are smaller.[27]

Interestingly, when comparing the fluorescence and excitation spectra,[36] we observe much larger shifts for fluorescence (see the larger slope in Figure 5). This is attributed to solvent relaxation occurring after excitation, and before emission takes place (probably on the fs time scale). These nuclear rearrangements make the ROH···**S** bond stronger, and therefore more sensitive to the solvent properties. One possibility is that the HB length shrinks in the ES.

TABLE 1: Kamlet−Taft Coefficients (cm^{-1}) for Two Dye Molecules in the Acid and Anion Forms[16,27]

	S_0			S_1		
molecule	$-p_0$	$-b_0$	a_0	$-p_1$	$-b_1$	a_1
2OH acid	70	510	270	450	800	0
2OH anion	0	0	3100	0	0	1770
5CN acid	150	680	270	1600	1950	0
5CN anion			?	0	0	940

SCHEME 6: Two Types of Hydrogen Bonds to 2OH[a]

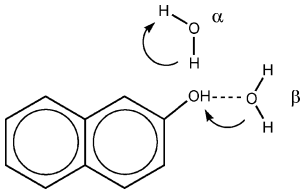

[a] α breaks and β becomes stronger upon excitation, as deduced from the corresponding Kamlet−Taft α and β parameters.

To verify this conclusion, we have also performed a multilinear regression of the ROH spectral shifts, ν_i, to the Kamlet−Taft equation[34]

$$\nu_i = \nu_{i0} + p_i\,\pi^* + b_i\,\beta + a_i\,\alpha \qquad (3.2)$$

where $i = 0$, 1 refers to the excitation (S_0) and emission (S_1) spectra, respectively. The two additional Kamlet−Taft parameters here are π^*, which is a measure of dipolarity effects, and α, which measures the HB-donating propensity of a protic solvent. The coefficients p_i, b_i, and a_i reflect *solute* properties in the *i*th electronic state: p_i is related to its dipole moment, b_i measures its propensity to *donate* a HB, and a_i describes its tendency to *accept* a HB from the solvent in the given electronic state. These parameters are summarized in Table 1.

Conclusions. Several interesting conclusions follow from this analysis.[15,16,27]

(a) ν_{i0} in eq 3.2 is the frequency for a solvent (such as cyclohexane) for which $\pi^* = \alpha = \beta = 0$. $\nu_{00} = 29\,400$ cm^{-1} (excitation) and $\nu_{10} = 28\,200$ cm^{-1} (emission). Thus fluorescence is red-shifted with respect to absorption already in the absence of these solvent effects, $\nu_{10} < \nu_{00}$. This contrasts with the situation for 8-hydroxypyrene-1,3,6-trisulfonate (HPTS), where $\nu_{10} > \nu_{00}$.[37] The latter was attributed to a $S_1 \leftrightarrow S_2$ level inversion. By this criterion there is no level inversion in 2OH and its cyano derivatives.

(b) The values of the p_i's are negative (red shift) and $|p_1| \gg |p_0|$, indicating an increase in the dipole moment upon excitation.

(c) The values of the b_i's are similar to the slopes of the two lines in Figure 5. In particular, both are negative (red shift) and $|b_1| > |b_0|$, suggesting charge migration from the OH, which is followed by shortening of the ROH···**S** bond. $b_0 - b_1$ is similar in magnitude to $p_0 - p_1$, suggesting that this single HB contributes about as much as nonspecific solvation from all other solvent molecules to the stabilization of the R*OH species.

(d) The a_0 parameter is small (and positive) for protic solvents (H**S**), whereas a_1 vanishes for the fluorescence spectrum. This suggests a weak RHO···H**S** bond to the hydroxyl oxygen in the GS, which cleaves in the ES.

The ensuing HB rearrangements following ROH excitation in water are summarized in Scheme 6. In the GS, two HBs exist: (i) A strong ROH···OH_2 bond and (ii) a weak RHO···

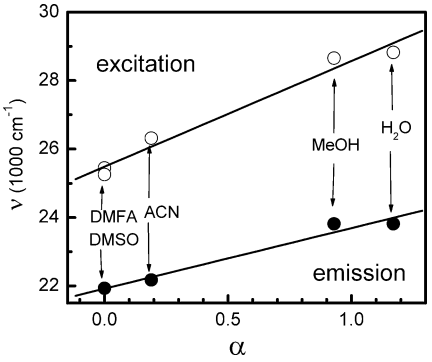

Figure 6. Solvatochromism of the naphtholate base correlates exclusively with the Kamlet−Taft α parameter, to which there is greater sensitivity in the excitation[36] than in the emission spectrum.[27] Data from ref 11. Solvent abbreviations as in Figure 5.

HOH bond. Commensurate with the decrease in electronic charge on the oxygen atom, the first HB becomes shorter and stronger in the ES, whereas the second one cleaves. Thus the ICT effect induces changes in HB strengths, probably occurring on the fs time scale.

Independent Verification. Several independent observations support the above scenario:

(a) Ab initio calculations on phenol-water clusters[38] find a short ROH···OH_2 bond (1.97 Å) and a longer RHO···HOH bond (2.12 Å). Moreover, upon excitation to S_1, the first one shortens whereas the second one lengthens (by 0.01 Å).

(b) In a series of combined spectroscopic/ab initio studies of gas-phase clusters (2OH···NH_3,[39] 1OH···NH_3,[40,41] hydroquinone···NH_3,[42] 7-hydroxyquinoline···NH_3,[43,44] and 7-hydroxyquinoline···OH_2[45]), the R*OH···NH_3 or R*OH···OH_2 bonds all appear to shorten upon excitation to S_1, typically by 0.01−0.1 Å.

(c) A similar effect is observed in intramolecular ESPT within hydroxyanthraquinones, where the O···O HB shrinks by 0.12 Å or more upon excitation to S_1.[46,47]

(d) Time-resolved IR studies of coumarin-phenol mixtures in methylene chloride,[48,49] revealed the cleavage of the HB donated from phenol to the carbonyl oxygen of the coumarin in the sub-200 fs time scale.

B. RO^- Solvatochromism. ICT plays an even larger role in stabilizing the anion, where a full negative charge on the oxygen needs to be dispersed.

(a) Unlike the acid, where the main stabilization effect is due to HB accepting solvents (Kamlet−Taft β parameter), here it is due to HB-*donating* solvents (Kamlet−Taft α parameter). Protic solvents (H**S**) stabilize the anion by forming a RO^-···H**S** bond, so that the solvatochromic shifts for 2-naphtholate correlate exclusively with the Kamlet−Taft α parameter.[27] This correlation is shown in Figure 6, with the a_i parameters given in the second line of Table 1.

(b) The a_i's for the naphtholate base are very large. The stabilization of the anion amounts to thousands of wavenumbers, as compared with hundreds of cm^{-1} for the ROH acid.

(c) As opposed to the acid, where a larger β parameter leads to a red shift, in the anion the shift with increasing α is to the blue. Hence stabilization by the RO^-···H**S** bond is more important in the GS than in the ES. This follows because of the decrease in the ES charge density on the O^- site.

(d) As opposed to the acid, where the sensitivity to β is much larger in the emission spectrum, for the base the sensitivity to α decreases significantly in the emission spectrum (as compared with the excitation spectrum). This must then indicate that the RO^-···H**S** bond is shorter in the GS and thus becomes *longer* upon excitation. Moreover, the effect is more pronounced than the shortening of the ROH···**S** bond upon excitation of the acid and should thus be easier to detect by complementary methods.

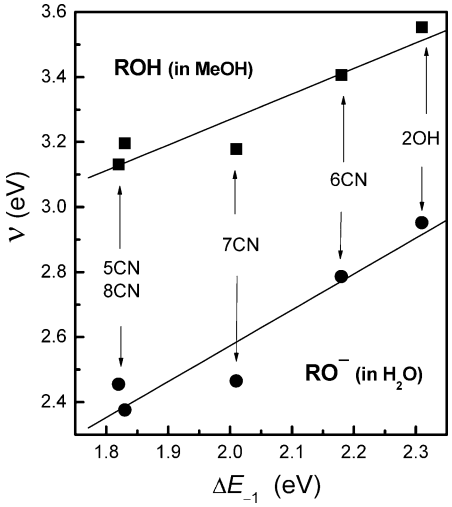

Figure 7. Fluorescence band position for cyano-2-naphthols: R*OH in methanol (Figure 4 of ref 17) and R^*O^- in water (Table 1 of ref 12), plotted as a function of the calculated $S_0 \leftarrow S_1$ energy gap for optimized S_1 of the corresponding gas-phase anion (Table 2 and Figure 1 of ref 29).

C. Substituent-Induced Spectral Shifts. Substituents on the aromatic rings lead to spectral shifts that may serve as a probe for the electron density at the substitution site. Figure 7 shows the cyano substituent effect on the peak emission frequency, ν, of the 2OH acid and anion forms in solution. In the first case the solvent is methanol, because in water the more acidic compounds are fully dissociated. In the second case the solvent is water, because in methanol the least acidic compounds do not dissociate (see Figure 4 in ref 17). It is difficult to find one solvent in which both fluorescence peaks are observable for all five compounds.

It is seen that the introduction of an electron-withdrawing substituent into the distal ring of 2OH induces a large red shift, particularly for the anion. This indicates that the substituent stabilizes the ES more than the GS, in accord with the ICT ansatz that electron density moves to the distal ring in the ES. The shift is largest for the most acidic 5CN and 8CN molecules, in agreement with the electronic charge density in Figure 4 and the experimental pK_a^* values in Scheme 3. (An exception is 7CN, for which the red-shift is larger than expected from its pK_a^* value.)

Additionally, Figure 7 shows that the substituent-induced spectral shifts correlate in both cases with the calculated $S_0 \leftarrow S_1$ energy gap, ΔE_{-1}, in the gas-phase *anion*, which is largest for the least acidic 2OH derivative. For the anion, the gas-phase ΔE_{-1} is always *smaller* than the solution-phase frequency ν, because the polar solvent stabilizes the GS more than the ES, in which the charge is more dispersed due to the ICT effect. However, the variation with substituent is nearly identical (slope of 0.9). Thus the ICT effect appears to be of similar magnitude for isolated and solvated anions.

The behavior of the acid is somewhat surprising because from the gas-phase calculations (section II) no correlation is expected. The $S_0 \rightarrow S_1$ energy gap is identical within computational error for all cyano substituents (Table 2 of ref 29), and no net charge was found to migrate to the distal ring. This result is indeed in better qualitative agreement with gas-phase experiments: Gas-phase 2OH has two rotamers, trans and cis, depending on the OH orientation with respect to the naphthalenic ring. Their 0−0

transitions occur in the absorption spectrum at 3.792 and 3.831 eV, respectively.[50,51] From the R2PI spectrum of 5CN, the values of 3.698 and 3.736 eV were obtained for the 0−0 transitions of the trans and cis rotamers, respectively.[52] Thus the red shift in the gas-phase ROH spectrum (ca. 0.1 eV) does appear to be small in comparison to that in liquid MeOH (ca. 0.4 eV; see Figure 7).

The fact that the solution-phase frequencies for R*OH fluorescence are found to correlate with the calculated gas-phase energies of the RO^- suggests that, *in solution*, the ICT effect occurs already for the acid form (although it is weaker than for the anion). Thus one should be careful when projecting from gas-phase calculations to solution to conclude[26] that the literature is wrong in suggesting ICT for ROH. It is better to reserve judgment until the solvent is explicitly included in the quantum calculations.

The substituent effect on the acid form is also evident by comparing the solvatochromic parameters b_i for 2OH and 5CN in Table 1. The 5-cyano substituent increases $-b_0$ by only about 30%, whereas $-b_1$ increases by a factor of 2.4. Thus the electron-withdrawing substituent induces some contraction of the ROH···**S** bond in the GS, and a very significant contraction in the ES. This, again, would not be expected if there were no ICT for the acid.[26]

IV. The Dissociation Event

A central place is reserved in PT reactions for the elementary dissociation step, whose rate coefficient is denoted by k_d. This step occurs on the picosecond time scale, well after the HB rearrangements in the ES. One naturally asks what determines the magnitude of k_d for ESPT reactions? Is it governed by the covalent interactions within the proton-transferring complex or by the solvent conformation? To address this question, we consider below structure−reactivity correlations, inter- vs intramolecular rates, the dependence of k_d on water concentration, temperature, and isotopic substitution. From these considerations, it appears that when the PT reaction is slow it is controlled by the covalent interactions whereas when it is fast its rate is determined largely by solvent rearrangement.

A. Structure−Reactivity Correlations. For a "family" of PT reactions, $AH + B \rightleftharpoons A^- + BH^+$, Brönsted and Pedersen[53,54] noted that the free energy of activation, $\Delta G^\dagger$, correlates rather nicely with the free energy of reaction, ΔG. Certainly when the reaction is endothermic, this "driving force" for reaction reflects the difference in the covalent bond strengths, between the product BH^+ bond and the reactant AH bond. Thus the more downhill the reaction, the smaller the barrier and the larger the rate coefficient.

More quantitative "structure reactivity correlations" for PT reactions were later developed by Marcus[55,56] on the basis of the empirical bond-energy−bond-order (BEBO) model,[57] and by Agmon and Levine[58−60] from a mixing entropy argument. Given an "intrinsic barrier" parameter, $\Delta G_0^\dagger \equiv \Delta G^\dagger(\Delta G{=}0)$, the correlation may be written as

$$\Delta G^\dagger = \Delta G - \Delta G_0^\dagger \ln(n^\dagger)/\ln(2) \tag{4.1a}$$

$$n^\dagger = [1 + \exp(-\Delta G \ln(2)/\Delta G_0^\dagger)]^{-1} \tag{4.1b}$$

The "Brönsted coefficient", $n^\dagger$, is the fractional bond order of the product, BH^+ bond, at the transition state (TS). When it is small, the TS is "early" (typical of exothermic reactions) whereas when it is large, the TS is "late" (typical of endothermic reactions). Following Pauling,[61] the bond order (BO), n, is related exponentially to the bond length, r,

$$n = \exp[-(r - r_{eq})/a] \tag{4.2}$$

where r_{eq} is its equilibrium value and a an empirical parameter. The dissociation rate coefficient is subsequently given by

$$k_d = k_d^0 \exp(-\Delta G^\dagger/k_B T) \tag{4.3}$$

so that it is controlled by the two kinetic parameters, k_d^0 and $\Delta G_0^\dagger$, and the thermodynamic "driving force" for the reaction, ΔG.

Unlike the situation for electron-transfer reactions, the above expressions do not show an "inverted" behavior. Thus k_d increases monotonically with increasing driving force ($\Delta G \rightarrow -\infty$): $\Delta G^\dagger \rightarrow \Delta G$ when $\Delta G \rightarrow \infty$, whereas it tends to zero as $\Delta G \rightarrow -\infty$. In general, there is scarce experimental evidence for the inverted region in PT reactions. The two known exceptions[62−64] occur in nonaqueous solutions and do not involve ESPT from the singlet state.

Structure−reactivity correlations for ROH photoacids have been depicted in several publications,[6,16,65−68] some of which utilize the above relations to fit their data (see original publications for figures). They do not show an inverted behavior. Typical values for the kinetic parameters are[67] $\Delta G_0^\dagger = 1.6$ kcal/mol, and $k_d^0 = 2.5 \times 10^{11}$ s^{-1}. The intrinsic barrier is rather small, which may again suggest that the barrier occurs mainly along the solvent coordinate.

More elaborate structure−reactivity correlations include the intersecting state model (ISM), which has recently been applied to ESPT from naphthol derivatives.[68] This model is based on intersecting Morse curves with "dressed" Morse parameters, reflecting the effect of the B moiety on the AH bond (and vice versa). Again, rather good agreement with experiment was demonstrated. Another recent extension introduces the solvent coordinate explicitly as the reaction coordinate.[69,70] This approach should be useful for ESPT, in which the solvent plays a dominant role.

B. Inter- vs Intramolecular PT. The "ultimate" ($\Delta G \rightarrow -\infty$) intermolecular ESPT rate constant, k_d^0, corresponds to a time-constant of about 4 ps. This is slower than typical values for fast intramolecular ESPT[10,71−74] by a factor of nearly 100. In the limit that the PT potential is barrierless, the intramolecular reaction is thought to be modulated by the heavy atom vibration (AH···B). For example, in jet-cooled (gas-phase) methyl salicylate, Zewail and co-workers[10] have observed barrierless intramolecular ESPT occurring within 60 fs. They have also observed a low-frequency, 180 cm^{-1} progression, which they attribute to bending of the OH···O bond. (Its half-period of 90 fs is consistent with the 60 fs time scale of the ESPT). Similarly, solution-phase femtosecond pump−probe measurements by Elsaesser and co-workers[73] have identified a 470 cm^{-1} mode, which is thought to modulate the heavy-atom distance along the active OH···N bond, leading to an intramolecular ESPT time of 60−80 fs. Theories for vibrationally assisted PT,[75−78] in their simplest form, predict that the rate constant in eq 4.3 gets multiplied by

$$\exp\left[\alpha_0 \coth\left(\frac{\hbar\omega}{2k_B T}\right)\right] \tag{4.4}$$

where ω is the frequency of the promoting heavy-atom mode, and α_0 is a constant.

Returning to intermolecular ESPT, Rini et al.[79] have used femtosecond time-resolved IR techniques to follow the reaction of HPTS with an acetate ion (B^-). At high acetate concentrations, they have observed an ultrafast component, faster than their 150 fs resolution, which they attribute to a direct reaction within a preformed ROH···B^- complex. This component is thus as fast as intramolecular ESPT, whereas a slower, truly bimolecular component, proceeds in the picosecond time scale. The distinction, then, is not between intra- and intermolecular reactions, but rather between donor−acceptor pairs that are already connected through a HB when excited or not. When they are, the reaction can be less than 100 fs and controlled by modulations of the OH···O distance.

It remains to consider the apparent "upper limit" to k_d for the truly bimolecular PT reactions. Rini et al.[79] interpret their results as implying that these reactions are limited by desolvation of the donor and acceptor, to form a directly H-bonded pair. This resembles the "inner sphere" mechanism for electron-transfer reactions. Slow PT reactions may proceed via such a mechanism, but these are controlled by cleavage of the covalent bond rather than by solvent dynamics.

For fast PT reactions the alternative "outer sphere" scenario may be more plausible. In this scenario the intimate PT step occurs when the donor and acceptor are separated by one or two water molecules. Indeed, proton diffusion is about 4 times faster than the self-diffusion of water.[80,81] It is thus faster to shuttle the proton than move away the intervening water molecule. The presence of the donor and acceptor accentuates the effect, because the lifetime of a water molecule in the first solvation shell of an ion is larger than in the bulk,[82] whereas the proton may be driven faster than in the bulk by a donor−acceptor potential gradient.

Consequently, the rate limiting solvent rearrangements are likely to be those that are required to solvate the products of the PT reaction. In particular, for ESPT to solvent from ROH photoacids most of the attention should be devoted to solvating the *anion*. This may be understood in terms of Scheme 6: The HB donated by the OH moiety becomes stronger upon excitation, whereas the one donated to it possibly cleaves. This advances that proton along its reaction coordinate but retards the solvation of R*O^-. To induce dissociation into ions, there is need to increase the coordination number of the anion by re-forming the cleaved HB.[83] This may require more extensive solvent rearrangements than anticipated in GS simulations of acid dissociation.[84,85]

C. Dependence on Water Concentration. Additional evidence for solvent involvement in the dissociation step comes from a study of ESPT to methanol−water mixtures.[17] Figure 8 shows that the dissociation rate coefficient depends on a power, w, of water concentration over a wide concentration range

$$k_d = k_m + k_w[H_2O]^w \qquad (4.5)$$

and for various photoacids. Here k_m is the dissociation rate coefficient for pure methanol. It is 0 for the three weakest photoacids, which are not capable of transferring a proton to methanol. Both k_m and k_w increase with photoacidity. A similar relation was observed earlier[86] for the decrease of k_d with added inert salt (in the molar range). In the latter case the correlation is universal (independent of the chemical identity of the ions) if the *activity* of water, rather than its concentration, is used.

The first interpretation of the power w was as the number of water molecules solvating the dissociated proton. Robinson and collaborators[87,88] suggested that four water molecules (4WM) are required to form the Eigen cation, $H_9O_4^+$. This interpretation has some difficulties. First, we find values of w roughly between 1 and 2, not 4 as suggested in the 4WM. Second, w is not constant but depends on the photoacid. Figure 9 shows a correlation of w with pK_a^*: The weaker the photoacid the larger w. The 4WM would predict that w, as a property of the equilibrated proton, should be independent of the conjugate base. Finally, the free energy of transfer of a proton (from water to the mixture), as deduced from extra-thermodynamic data, is nearly independent of solvent composition in the water-rich region.[89] Though the proton "sits" on one water molecule, water and methanol are equally probably as its first-shell ligands.

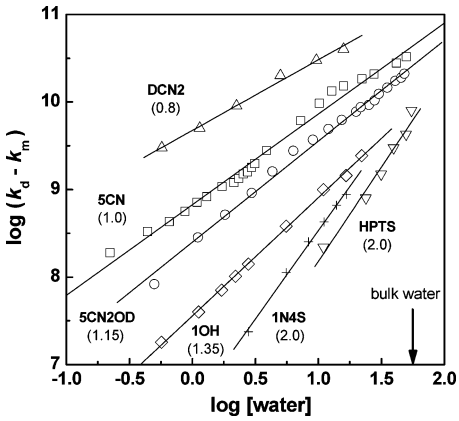

Figure 8. Dependence of the proton dissociation constant (in s^{-1}) on water concentration (in M) in methanol/water mixtures for six ROH photoacids in their S_1 state. Data from Figure 12 of ref 17, with new linear fits spanning the whole concentration range. In parentheses are the values of w fitted to eq 4.5.

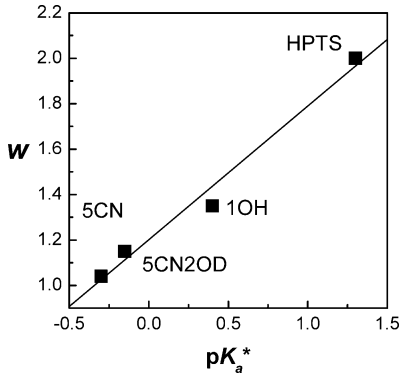

Figure 9. Dependence of the water power w (see Figure 8) on the photoacid strength.

It appears from Figure 8 that the smallest value of w is around 1, because w does not change appreciably between DCN2 ($pK_a^* = -4.5$) and 5CN ($pK_a^* = -0.8$). The $w = 1$ limit may correspond to the single water molecule on which the proton resides. For the weaker photoacids, w increases linearly with increasing pK_a^*. The weaker the photoacid the smaller the ICT effect and hence the larger the negative oxide charge that needs to be solvated. Because the Kamlet−Taft α parameter is larger for water than for methanol, water will be more effective in solvating the nascent anion. Thus weak photoacids may require additional water molecules in the solvation shell of their conjugated photobases to assist in the dissociation process.

D. Temperature Effect. Another indication that fast ESPT reactions are solvent controlled comes from the unusual temperature effect on k_d. Weak photoacids, like 2OH, behave in an Arrhenius fashion, with ln k_d linear in $1/T$ between the freezing and boiling temperatures of water.[87,88,90] Its activation enthalpy is $E_A \approx 11$ kJ/mol. There is some downward deviation

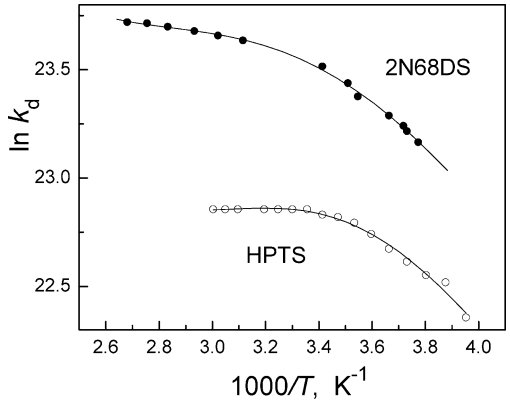

Figure 10. Dependence of the dissociation rate coefficient (in units of s^{-1}) on temperature, for two photoacids. Data from refs 92 (HPTS) and 90 (2N68DS). Lines show fourth-order polynomial fits, which were differentiated analytically to give E_A.

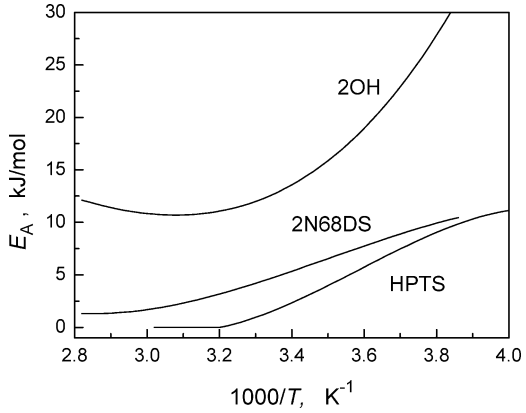

Figure 11. Dependence of the activation energy on temperature for the deprotonation of three different photoacids. Obtained by differentiating the polynomial fits shown in Figure 10.

from the Arrhenius behavior only in supercritical[91] or supercooled water.[90] In contrast, stronger photoacids such as HPTS[92] or 2-hydroxynaphthalene-6,8-disulfonate (2N68DS)[90] in water, and the superstrong DCN2 in alcohols,[93] exhibit a strongly curved Arrhenius plot. This behavior is demonstrated for ESPT to water in Figure 10, with the extracted activation enthalpies shown in Figure 11. These results depend delicately on the polynomial chosen to fit $k_d(T)$ in Figure 10, which was then differentiated analytically to give E_A. Yet, qualitatively, it is clear that E_A *increases* with decreasing T.

This behavior contrasts with the temperature dependence expected from theories of nonadiabatic PT, where k_d is controlled by proton tunneling.[75−78] For example, the hyperbolic cotangent term in eq 4.4 suggests that E_A *decreases* with decreasing T, which is just the opposite of the observation in Figures 10 and 11. This suggests that ESPT to solvent is controlled by the adiabatic motion of the solvent, whereas proton tunneling plays a relatively minor role.

Robinson and co-workers[87,88] have suggested that the solvent controls k_d via the Debye dielectric relaxation time, τ_D. This explanation is too simplistic because, around room temperature, k_d has a much weaker temperature dependence than $1/\tau_D$.[92] Consequently, Huppert and collaborators[90,92,93] have suggested a switch between solvent control ($1/\tau_D$ behavior) at low temperatures and proton tunneling at the higher ones.

Yet if we consider the two stronger photoacids in Figure 11 we notice that they have $E_A \approx 0$ at high temperatures, suggesting a negligible barrier along the proton coordinate. Moreover, $E_A(T)$ seems to depend relatively little on the photoacid in this

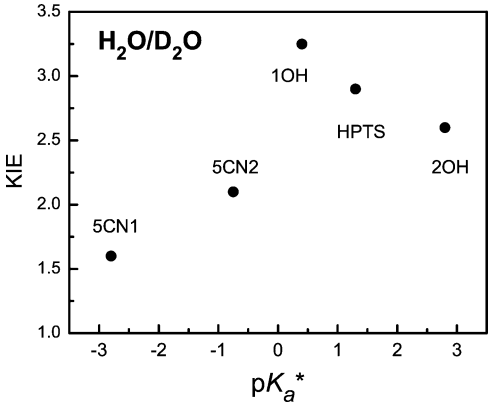

Figure 12. Dependence of k_d^H/k_d^D on the thermodynamic driving force for ESPT from a series of photoacids to water at room temperature. Data are conveniently collected in Table 3 of ref 68, except that the KIE for HPTS is 2.9 and for 5CN2 it is 2.1.

limit. Thus it may be more plausible to assume that *the whole* temperature dependence is controlled by the solvent. This contrasts with the weaker 2OH, which has a large and nearly T-independent E_A above 0 °C, attributable to a barrier in the proton coordinate. Below 0 °C, the rise in its E_A appears to be more dramatic than for the faster photoacids, commensurate with our assertion that more water molecules are needed to solvate the anion of a weaker photoacid.

E. Kinetic Isotope Effects. The kinetic isotope effect (KIE) is defined as the ratio of the rate constants (k) without and with isotopic substitution. Most common is the H/D KIE, defined as k^H/k^D. In ESPT to water, k_d^H/k_d^D, is the ratio of the dissociation rate coefficient in H_2O and D_2O.

Many years ago Melaner[94] and Westheimer[95] have suggested that, within a reaction series, the KIE should exhibit a symmetric maximum when $\Delta G = 0$. Such behavior can be obtained from the structure−reactivity correlations, e.g., eqs 4.1, if only $\Delta G_0^{\ddagger}$ varies with isotopic substitution.[58−60] The correlation may be nonsymmetric if also ΔG is isotopically dependent, as observed for the H_2 + X series (X a halogen atom).[96] In this case the KIE decreases faster for negative ΔG values. Interestingly, the same asymmetry is observed for ESPT to water in Figure 12, although the data here are less accurate so it is difficult to say what is the origin of its asymmetry.

Theories for nonadiabatic, tunneling-controlled PT suggest that the KIE should be large (e.g., 5−50) and depend only weakly on temperature, possibly in an Arrhenius fashion.[97] Figure 13 shows the KIE for the dissociation of excited HPTS in water. It is relatively small and depends on temperature more strongly as T is lowered. This discrepancy indicates, again, that proton tunneling plays a minor role is ESPT to water, so that the observed KIE may have a large contribution from the HB dynamics of water molecule clusters surrounding the excited probe.

V. Proton Mobility

The dissociation process generates a solvated proton that diffuses in solution. The diffusion constant of a proton in water, ca. 9.3×10^{-5} cm^2/s at room temperature, is at least 4.5 times larger than any other cation.[98] The proton hopping time has been measured independently using NMR techniques to be in the range of 1−2 ps.[99] The origin of the abnormally high proton mobility is attributed to the "Grotthuss mechanism",[100−102] whose exact nature has been a source of vivid controversies.[80] Understanding the mechanism of proton mobility in water is important beyond the immediate scope of ESPT, because protons

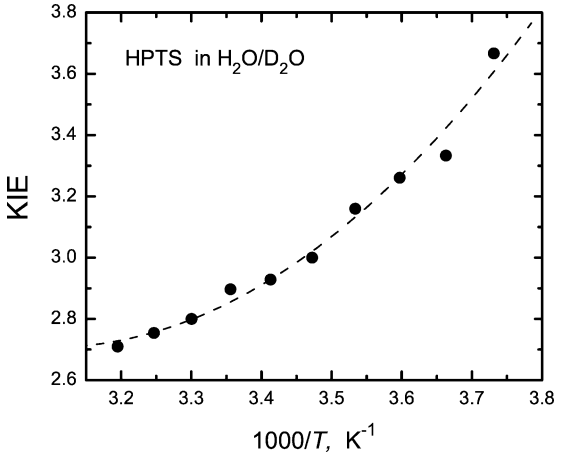

Figure 13. Temperature dependence of k_d^H/k_d^D for ESPT from HPTS to water.[92] The parabolic line is drawn to guide the eye and stresses the non-Arrhenius nature of these data.

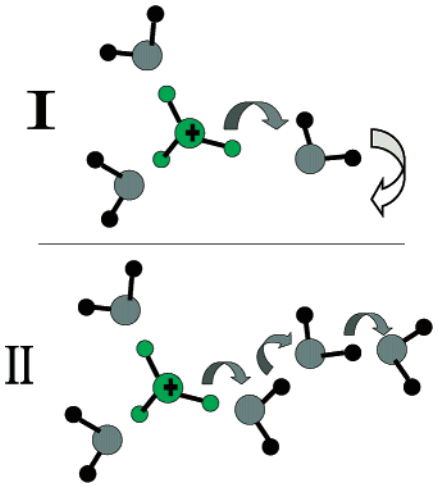

Figure 14. Classical models for proton hopping in water: (I) model of Bernal and Fowler;[103] (II) picture emerging from the work of Eigen and collaborators.[105] Small gray arrows indicate proton hops, whereas the large white arrow denotes water rotation.

catalyze an immense number of aqueous reactions and serve as a means for transient energy storage in living systems.

A. Existing Models. Figure 14 summarizes some classical concepts concerning the mechanism. (I) shows the scenario of Bernal and Fowler,[103] in which a water molecule rotates in the vicinity of the H_3O^+ cation. When it achieves the correct orientation, the proton hops on. (II) is based on the interpretation by Eigen and DeMaeyer of their studies of proton mobility in ice.[104,105] Because proton was found to migrate faster in ice than in liquid water, they proposed rapid proton dislocations along chains of H-bonded water molecules. These two concepts were combined into a single textbook picture.[106]

The above concepts were criticized,[80,81,107] on the basis of several arguments:

1. First-shell HBs to H_3O^+ should not typically be broken, because they are shorter and stronger than ordinary water−water HBs.

2. The activation energy for proton mobility is low, about 2.5 kcal/mol at room temperature.[98] It is similar to the HB strength between water molecules, 2.6 kcal/mol, as deduced from Raman studies.[108] Thus a rate determining step must involve the cleavage of ordinary water−water HBs further away from the protonated center.

3. The activation energy for proton mobility increases steeply in supercooled water, even though the HB network becomes more ordered.[81] The effect indicates cooperative rearrangement of HBs, which necessitates several concerted cleavage events.

4. Proton mobility in ice is actually *slower* than in supercooled-water of the same temperature.[109,110]

5. Coherent-like proton hopping along preformed chains of HBs is not likely, because the coordination number of liquid water is too high (near 4). To become H_3O^+, the coordination number of the proton-accepting water molecule should first decrease to 3.

6. The proton diffusion coefficient at room-temperature is $D_{H^+} = 9.3 \times 10^{-5}$ cm^2/s. This value is reproduced well by Einstein's relation

$$D_{H^+} = l^2/6\tau_{H^+} \tag{5.1}$$

where $\tau_{H^+} \approx 1.2$ ps is the proton hopping time as determined by NMR,[99] and $l \approx 2.6$ Å is the distance between H_3O^+ and the oxygen atom in its first solvation shell.[111] This indicates that proton hops are incoherent, with long intervals between hops during which memory of where the proton came from is lost.

7. The unique role ascribed to the strongly solvated H_3O^+ cation, designated by Eigen as $H_9O_4^+$,[105] has been contested by Zundel,[112,113] who found a broad IR continuum in aqueous solutions of strong acids. This he attributed to proton fluctuations within the protonated water dimer, $H_5O_2^+$. Both cations[114] are observed in simulations of protonated water, as depicted in Figure 15.

Following these considerations, it was clear that revised models for proton mobility were required. The next-generation models arrived in 1995.[80,115] The two models depicted in Figure 16 are characterized by nearly isoenergetic Eigen and Zundel cations.[114] Proton moves by rapid interconversion of these cations, which are driven by second-shell HB dynamics. In mechanism I, the Zundel cation is dominant, and protons hop by a double-proton translocation that converts one Zundel cation into another.[115−117] In mechanism II,[118] the more stable Eigen cation is transiently converted into a Zundel cation by cleavage of a HB donated to the acceptor oxygen atom.[80] A new Eigen cation is stabilized on the acceptor side, by forming a HB to the donor oxygen. This picture was confirmed by Car−Parrinello simulations[119] and found its way into textbooks.[120] A related scenario was discovered in MD simulations of proton mobility in ice.[121]

However, mechanism II still has its problems. Using multi-state empirical valence-bond (MS-EVB) potentials,[122] efforts were made to observe the suggested HB cleavage that supposedly reduced the coordination number of the acceptor from 4 to 3.[116,123,124] An effect was found, but much weaker than expected. Possibly, the suggested HB cleavage event occurs more frequently in the *next* solvation shell.[124] But then there is more than one such bond to consider.

The reason for the discrepancy is that in mechanism II it is assumed that the first-shell water ligands behave like bulk water, possessing a coordination number around 4. This is not true for the MS-EVB potentials in which the three first-shell neighbors of the H_3O^+ ion participate in delocalizing around 30% of the positive protonic charge.[124] Consequently, it becomes electrostatically unfavorable to donate a HB to these oxygen atoms, leading to an average coordination number of 3.6, rather than 3.9 as in bulk water.[124,125] Because the HB that was suggested to cleave is not there 40% of the time, its cleavage

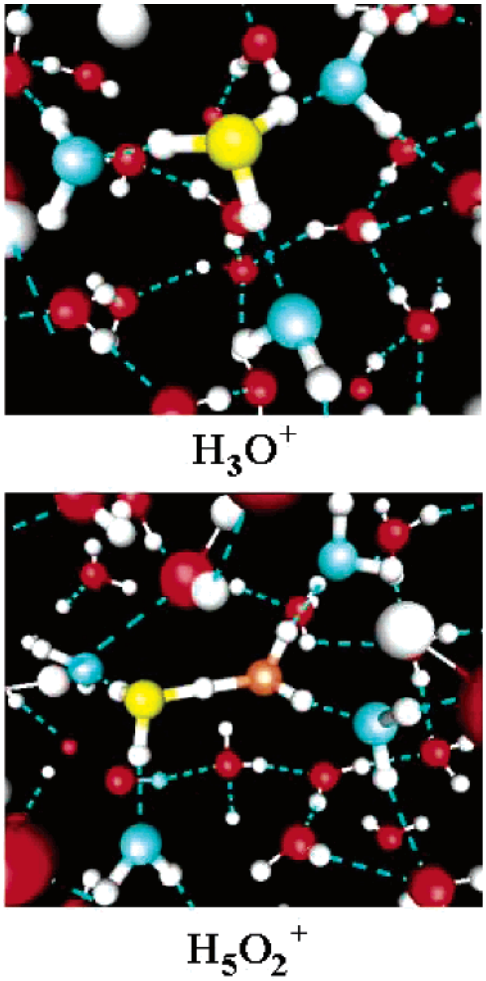

Figure 15. Eigen (yellow) and Zundel (yellow-orange) cations,[114] with their first solvation shells (cyan), as revealed in MS-EVB simulations of protonated water. HBs are denoted by dashed (cyan) lines. Calculation using the MS-EVB2 program of Schmitt and Voth[122,124] and the gOpenMol visualization software (Laaksonen, 2001).

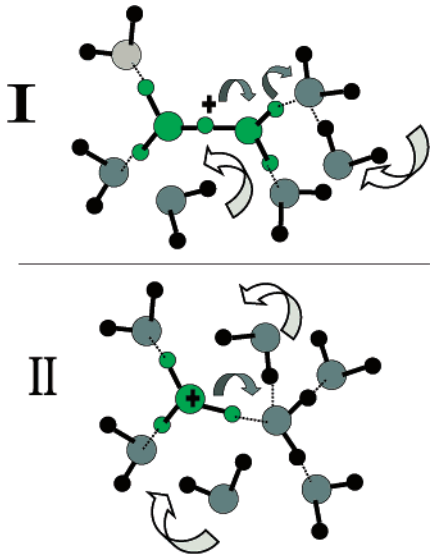

Figure 16. Recently proposed models for proton hopping in water: (I) Zundel-to-Zundel conversion;[115] (II) Eigen-to-Eigen conversion (via an intermediate Zundel cation).[80] In both cases, a HB to the acceptor side breaks, whereas an equivalent bond is re-formed with the donor by water rotation (large white arrows).

cannot be the rate-limiting step, and one should consider H-bonding effects in much larger water clusters.

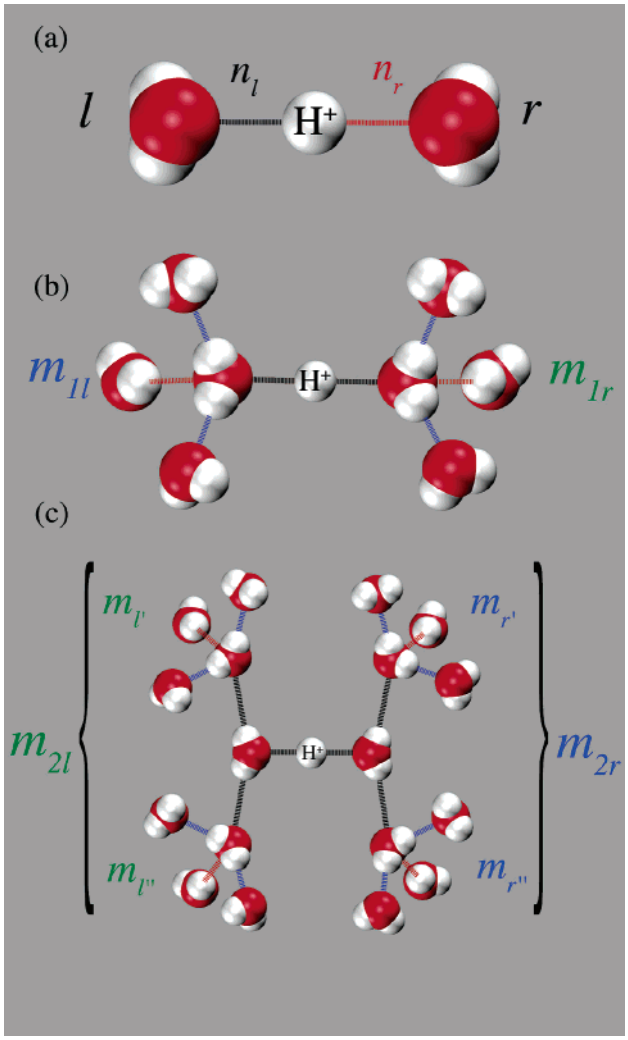

Figure 17. Proton-transferring complex, $H_5O_2^+$ (a), and its first two solvation shells. In the first-shell (b), six HBs are tracked. In the second-shell (c), 12 HBs are tracked. The two unfavorable HBs from the first shell (red) are not followed onto the second shell. Reprinted with permission from ref 126. Copyright 2004. American Institute of Physics.

B. Cooperative Picture of Proton Mobility. To investigate cooperative effects on proton mobility in liquid water, consider the first- and second-shell water clusters around the transferring $H_5O_2^+$ complex. Figure 17 shows two kinds of HBs participating in these clusters. The "good" bonds in blue around a given oxygen atom would stabilize a proton moving to it, whereas the "bad" bonds in red would destabilize it. The models in Figure 16 assumed that one bad bond is cleaved in the rate-limiting step. A recent MD study by Lapid et al.[126] indicates that also the good bonds participate, allowing the coordination number to drop below 3. This occurs in the second shell of the $H_5O_2^+$ complex, Figure 17c, so that larger protonated water clusters than previously anticipated participate in the PT dynamics.

To proceed, define the average proton reception power of a given oxygen center in terms of its HB environment, as[126]

$$m = n_1 + n_2 - n_3 \qquad (5.2)$$

Here n_i are BOs calculated from eq 4.2. The (maximum) of four HBs in which this oxygen participates are divided as follows: n_1 and n_2 represent the two good HBs it donates, whereas n_3 is the BO of the bad HB donated to it. Hence n_3 receives a negative weight in eq 5.2. The fourth HB is the one

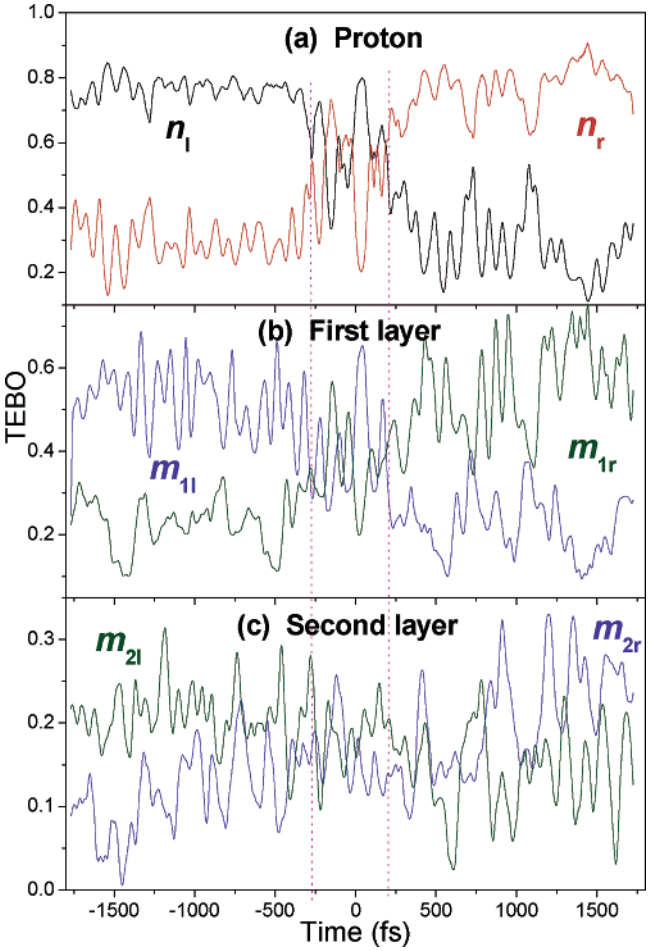

Figure 18. Proton-transfer dynamics correlates with the HB dynamics within the first two solvation layers surrounding the $H_5O_2^+$ complex. (a) depicts a PT event in the inner complex. The first and last crossings of n_l and n_r delimit the existence of the complex (vertical dashed lines). The zero of time is set at the middle of this interval. The two BO parameters in (a) and four TEBO parameters in (b) and (c) have been smoothed to eliminate fast hydrogen atom vibrations.

along which the proton moves; hence it is not counted in the HB environment. The parameter m is called the "total effective bond order" (TEBO). The larger its value, the more receptive the oxygen center toward the migrating proton.

With these definitions, one can characterize the HB environments in the three levels depicted in Figure 17. The inner $H_5O_2^+$ complex is characterized by the BOs n_l and n_r, for the donor (left) and acceptor (right). The TEBO parameters are used for characterizing the two solvation shells. For the donor and acceptor sides in the first shell we have m_{1l} and m_{1r}, respectively. In the second shell, there are two TEBO parameters on each side that are averaged to give m_{2l} and m_{2r}, respectively. These four TEBO parameters were calculated during each PT event using the MS-EVB2 simulation program.[124] This program calculates the potential quantum-mechanically using the best available MS-EVB parametrization, but the nuclear motion is classical.

As Figure 18 shows, PT between two water molecules is characterized by a transient formation of a Zundel cation, between the first and last times that $n_l = n_r$. Concomitant with it, the TEBO values of the two solvation layers also coincide. This behavior is typical for all the PT events investigated. From the behavior of the TEBO parameters we deduce several important characteristics of PT events (at least within the MS-EVB2 description):

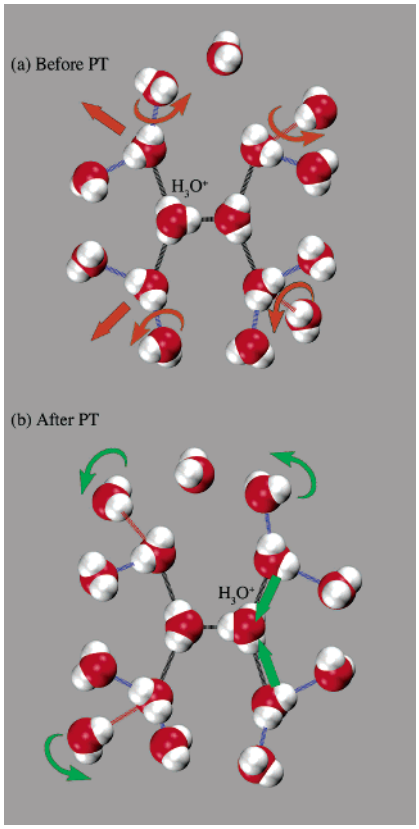

Figure 19. HB dynamics couples to proton mobility in water. (a) Before PT, "good" HBs may break (curly orange arrows) on the donor side (left) whereas "bad" ones break on the acceptor side (right). Several such events tilt the balance from donor to acceptor. (b) After PT, HBs form in the second solvation shell (curly green arrows). "Good" HBs form on the acceptor side and the "bad" ones form on the donor side. The first shell HBs around the $H_5O_2^+$ respond mainly by corresponding stretching/contraction translational motions. Reprinted with permission from ref 126. Copyright 2004. American Institute of Physics.

1. Changes in HB strengths occur collectively in both solvation layers.
2. Changes in the outer (second) layer possibly precede those in the first layer and the $H_5O_2^+$ complex.
3. Both bad and good HBs contribute to changes in the TEBO parameters. On the donor side, good bonds are broken and then bad bonds are formed. On the acceptor side, bad bonds are broken and then good bonds are formed.

A schematic summary of these HB dynamics is presented in Figure 19.

VI. Recombination and Quenching

The photoacid saga does not end upon dissociation and formation of a solvated diffusing proton. This proton can now participate in an adiabatic recombination reaction (eq 1.1) or in a nonadiabatic quenching reaction. These two reactions

$$R^*O^- + H^+ \xrightarrow{k_a} R^*OH \qquad (6.1a)$$

$$R^*O^- + H^+ \xrightarrow{k_q} ROH \qquad (6.1b)$$

are characterized by the rate constants k_a and k_q, respectively. They were first observed at low pH, where they occur with a homogeneous distribution of protons. Only more recently was it realized that they also occur with the geminate proton, which is the subject of the present section.

SCHEME 7: Suggested Proton-Quenching Mechanism for 2OH[25]

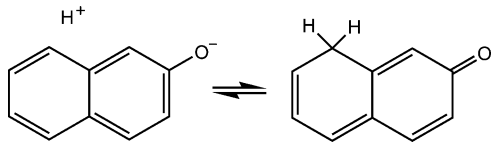

In the homogeneous case, the reversibility of ESPT to solvent was deduced by Weller from fluorometric titrations.[2] As the pH is lowered, the fluorescence band of the acid increases in intensity at the expense of the red-shifted anion band, ideally maintaining an isoemissive point. Laws and Brand have measured the reaction in the time domain, finding biexponential decay at low pH, which they attributed to reversibility.[127] Harris and Selinger suggested that nonadiabatic proton quenching is a major player in excited 1OH kinetics.[128] They found that both R*OH and R*O$^-$ are quenched by protons, with the latter a factor >10 faster. The larger charge on the distal ring of the anion may explain this result. Webb et al.[25] suggested that the dissociated proton attacks the distal ring at the position of highest electron density, followed by rapid crossing to the GS. For 2OH, this attack should occur at position 8; see Scheme 7. For 1OH it occurs at position 5 and k_q is about a factor 100 larger.

At neutral pH values, rebinding may occur with the *geminate* proton, leading to a nonexponential tail in time-resolved fluorescence measurements.[129] The behavior was explained quantitatively by a diffusion model described below.[130−132] The model has been extended to include geminate quenching *and* different ES lifetimes.[133−135] An account of this model, its numerical treatment, the major analytical results and a comparison with time-correlated single photon counting (TCSPC) fluorescence data are given below. The exposition shows how ESPT to solvent provides some of the most convincing examples of reversible diffusion-influenced reactions.

A. Diffusion Model. The diffusion model for ESPT to solvent,[131] is the simplest treatment of geminate reactions, which includes the effects of both translational diffusion and reversibility. To these were recently added the effects of quenching and different ES lifetimes.[133−135] In this model the anion is depicted as a sphere of radius a, with its total charge, z, at the center. The "contact distance" a is somewhat larger than the bare van der Waals radius, including at least the first solvation shell. z is the sum of the negative charge created by dissociation and those of all charged substituents (e.g., sulfonate groups). The solvent is assumed to be a homogeneous dielectric medium of static dielectric constant ϵ. Thus the Coulombic potential of interaction between the proton and the anion (in units of k_BT) at distance r is

$$V(r) = -\frac{R_D}{r} \qquad R_D \equiv \frac{|z|e^2}{k_B T \epsilon} \tag{6.2}$$

Here R_D is the Debye (or Onsager) distance (when $r = R_D$ the Coulomb interaction equals to the thermal energy), e is the electronic charge, and the proton charge is +1. Unlike some electrostatic treatments of proteins, we do not assume that the central sphere has a lower dielectric constant than the bulk, which would have introduced an added repulsion for the approaching proton. This may be justified because our sphere includes at least one solvent layer, and not just the bare organic molecule.

The relative diffusion coefficient D is the sum of the proton and anion diffusion coefficients. In practice, the anion diffusion coefficient (ca. 1×10^{-5} cm^2/s in room-temperature water) is often neglected, so that $D \approx D_{H^+}$. This neglect may compensate for a possible small reduction in proton mobility close to the anion.

The bimolecular reactions (dissociation, recombination, and quenching) are assumed to be isotropic, although there are clearly different proton binding sites involved. The justification for this is that rotational diffusion is rather fast, so that specific sites become "smeared" on the surface of the sphere. As a result the problem becomes spherical symmetric, depending on the single coordinate, r, but the fitted rate coefficients include the effect of a "steric factor". In addition, all three reactions are assumed to occur at $r = a$. In contrast to electrons or electronic excitations, which may hop coherently across large distances, the proton hops incoherently between adjacent water molecules (section V) until it hits the central sphere. Thus recombination and quenching are depicted by delta function "sink terms", $k_a\delta(r - a)/(4\pi a^2)$ and $k_q\delta(r - a)/(4\pi a^2)$, respectively. In contrast, the R*OH and R*O$^-$ ES decay constants (k_0 and k_0', respectively) are r-independent.

Mathematically, one considers the probability density, $p(r,t)$, for the pair to separate to a distance r by time t after excitation. The observed (normalized) signals from the excited acid and anion correspond to the protonation probability, $P(t)$, and the survival probability of the separated pair,

$$S(t) \equiv 4\pi \int_a^\infty p(r,t) r^2 \, dr$$

The population that has decayed to the GS is hence $1 - P(t) - S(t)$. $p(r,t)$ is assumed to obey a spherically symmetric Debye−Smoluchowski equation (DSE) in three dimensions, which is coupled to a kinetic equation for $P(t)$,

$$\frac{\partial}{\partial t} p(r,t) = \left[r^{-2} \frac{\partial}{\partial r} D r^2 e^{-V(r)} \frac{\partial}{\partial r} e^{V(r)} - k_0' \right] p(r,t) + [k_d P(t) - (k_a + k_q) p(r,t)] \frac{\delta(r-a)}{4\pi a^2} \tag{6.3a}$$

$$\frac{\partial}{\partial t} P(t) = k_a p(a,t) - (k_d + k_0) P(t) \tag{6.3b}$$

When only the acid form is excited, these equations are subject to the initial conditions $P(0) = 1$ and $p(r,t) = 0$. Because reactions are depicted by the sink terms, a reflective boundary condition, $\partial\{\exp[V(r)]p(r,t)\}/\partial r = 0$, is imposed at $r = a$. This sink-term formulation is best suited for analytic work.

B. Numerical Solution to the DSE. The numerical methodology for solving this partial differential equation has been developed through several earlier publications[131,136−138] and will not be reviewed here. Today, the numerical solution may be conveniently obtained using the Microsoft Windows application for solving the spherical symmetric diffusion problem, SSDP ver. 2.66.[139] It allows for immediate graphical comparison with experimental data.

Several points should be remembered when fitting experimental data:

1. Contact reactivity should be represented as the appropriate boundary condition ("radiation", "back-reaction") at $r = a$, rather than as a delta-function sink.[130,131] The Chebyshev propagator[137] should then be used for these boundary-value problems.

2. The calculation should be checked for convergence with respect to the spatial grid and the location of the (artificial) outer boundary.

3. Logarithmically increasing time steps are best suited for diffusional problems. For strongly varying potentials a nonuniform spatial grid (increasing from $r = a$ outward) will better sample the potential.

4. The short time decay is controlled by k_d, whereas the intermediate behavior and the long-time tail are sensitive to k_a, D, and $V(r)$. The tail is enhanced by faster recombination, larger attraction, and slower diffusion.

5. To allow for a unique determination of the parameters, some of them must be extracted from independent measurements. Typically, one utilizes known experimental values for T, ϵ, R_D, and D. This leaves mainly the rate constants as adjustable parameters.

6. The long-time tail may be sensitive to the effect of experimental "artifacts", such as minute quantities of fluorescing impurities, and spectral overlap between the R*OH and R*O$^-$ bands. Measures should be taken to correct for these factors.

7. The short time behavior is strongly dependent on the instrument response function (IRF), which includes the effects of the laser pulse and detection system. The IRF should be measured in parallel to the data (ideally, both should have the same time origin) and convoluted with the calculated kinetics before comparison with experiment.

C. Analytic Approximation to the DSE. In the absence of a potential of interaction, $V(r) = 0$, an analytic solution to eqs 6.3 could be found,[140] even for different ES lifetimes and geminate quenching.[135] This solution is useful in cases where the dissociation products are neutral, for example, ESPT to solvent from protonated aminopyrene.[65] In ROH acids, there is typically an attractive potential of interaction that enhances the recombination. This case can be solved only approximately,[133,134] yet the long-time asymptotic behavior may still be obtained analytically. These solutions are summarized below. For details on the mathematical derivation the interested reader should consult the original papers.

It is useful first to define some effective rate constants and reaction radii. In the presence of a potential, an effective radius is defined by

$$a_{\rm eff} = \left(\int_a^\infty e^{V(r)} r^{-2}\, dr\right)^{-1} \tag{6.4}$$

It reduces to $a_{\rm eff} = a$ when $V(r) = 0$ and to

$$a_{\rm eff} = R_D/[1 - \exp(-R_D/a)] \tag{6.5}$$

for the Coulomb potential in eq 6.2.

Subsequently, one defines two diffusion-control rate constants,

$$k_D \equiv 4\pi D a_{\rm eff} \qquad k_{-D} \equiv k_D e^{V(a)} \tag{6.6}$$

for the association and separation directions, respectively. With these, in turn, one can define two steady-state "off" rate constants

$$k_{\rm off} = \frac{k_d\, k_{-D}}{k_a + k_{-D} + k_q} \qquad k_{\rm off}^q = \frac{k_d\,(k_{-D} + k_q)}{k_a + k_{-D} + k_q} \tag{6.7}$$

and two additional effective radii,

$$a'_{\rm eff} \equiv \frac{k_a\, a_{\rm eff}}{k_a + k_{-D} + k_q} \qquad a_{\rm eff}^q \equiv \frac{(k_a + k_q)\, a_{\rm eff}}{k_a + k_{-D} + k_q} \tag{6.8}$$

The approximate solution[133,134] to eqs 6.3 can subsequently written in terms of two roots of a quadratic polynomial that appears in the denominator of the approximate Laplace transform,

$$\sigma_\pm = \frac{k_{\rm off}\, a'_{\rm eff}}{2D}\left(-1 \pm \sqrt{1+\beta}\right) \tag{6.9}$$

Here β is the dimensionless parameter

$$\beta \equiv \frac{(k'_0 - k_0 - k_{\rm off}^q)4D}{(k_{\rm off}\, a'_{\rm eff})^2} \tag{6.10}$$

These roots enter into the special function

$$\phi(t;\sigma_\pm) \equiv e^{\sigma_\pm{}^2 Dt}\, \mathrm{erfc}(-\sigma_\pm\sqrt{Dt}) \tag{6.11}$$

where erfc(x) is the complementary error function for a possibly complex argument, x. The approximate protonation and separation probabilities are finally written as[133,134]

$$P(t) = \frac{e^{-k'_0 t}}{2}\left(\phi(t;\sigma_+) + \phi(t;\sigma_-) - \frac{\phi(t;\sigma_+) - \phi(t;\sigma_-)}{\sqrt{1+\beta}}\right) \tag{6.12a}$$

$$S(t) = \frac{e^{-k'_0 t}}{\sqrt{1+\beta}}\left(\frac{(1+\sigma_+ a_{\rm eff}^q)\,\phi(t;\sigma_+) - 1}{\sigma_+\, a'_{\rm eff}} - \frac{(1+\sigma_- a_{\rm eff}^q)\,\phi(t;\sigma_-) - 1}{\sigma_-\, a'_{\rm eff}}\right) \tag{6.12b}$$

Figure 20 compares the approximation from eq 6.12a with the exact numerical solution of eqs 6.3. For all practical purposes

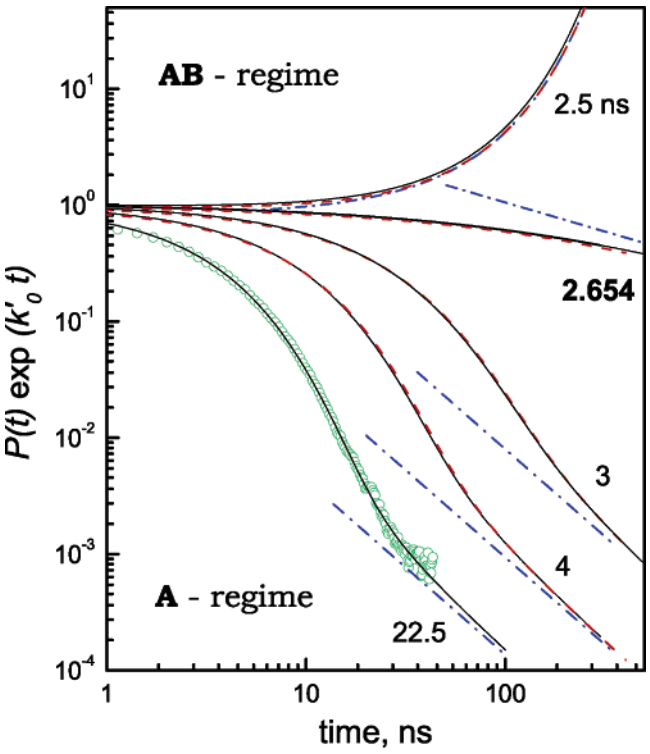

Figure 20. Protonation probabilities from the diffusion model of ESPT. Lines, calculated from the numerical solution of eq 6.3 using the SSDP software,[139] are compared with the approximation in eq 6.12a (red dashed lines) and the long-time asymptotics (blue dash−dot lines) in eq 6.13a below. Five sets of $1/k'_0$ values are applied, the largest fits the experimental data for ESPT from 5CN to DMSO (green circles).[16] Adapted from Figure 1 of ref 141. Parameters used: $a = 5.5$ Å, $R_D = 12.1$ Å, $D = 1 \times 10^{-5}$ cm^2/s, $k_a = 456$ Å^2, and $1/k_0 = 5.7$ ns.

SCHEME 8: Keto Resonance for the 5MS1M Anion Is Believed To Shorten Its ES Lifetime[13]

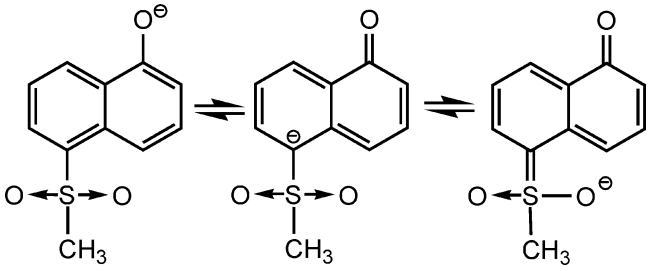

the agreement is excellent. The approximation is worse at short times, whereas at long times it converges to the exact asymptotic behavior, which will be discussed below.

D. Kinetic Transition. The asymptotic behavior can be deduced from the approximations in eqs 6.12, which become exact at long times, or directly from the Laplace transform of the DSE.[133,134] It undergoes a "kinetic transition",[141] depending on the sign of β defined in eq 6.10. Focusing on $P(t)\exp(k_0't)$, one finds two regimes with a sharp transition between them, characterized by the following asymptotic behavior

1. $\beta < 0$, $t^{-3/2}$ decay
2. $\beta = 0$, $t^{-1/2}$ decay
3. $\beta > 0$, exponential growth

These three types of behaviors are depicted in Figure 20, where the transition occurs for $1/k_0' = 2.654$ ns.

For a general dissociation-association reaction of the type AB $\rightleftharpoons$ A + B, with two different lifetimes for AB and A, this behavior can be understood as follows. Due to dissociation, AB decays at long times with the effective rate-constant $k_0 + k_{off}^q$, whereas A decays at long times only by k_0'. These two effective rate coefficients are exactly balanced at the transition, $\beta = 0$. When AB decays faster than A ($\beta < 0$), the reactive system is most of the time in state A, hence the term "A regime". This is the usual case in ESPT to solvent. Here diffusion effects have time to evolve, leading to the asymptotic $t^{-3/2}$ power-law decay. It reflects the probability of the A−B pair to return to the origin of their random walk (the normalization factor of the Gaussian solution for free diffusion in three-dimensions).

When A decays faster than AB ($\beta > 0$), there is no time for diffusional effects to accumulate, and the decay becomes exponential. In this case the system is most of the time in the AB state, so it is termed the "AB regime". It was nevertheless unexpected that a sharp transition should occur at a finite value of β and, moreover, that it could be observed experimentally.

To verify this transition experimentally, we searched for ROH dyes with particularly short anion lifetimes. 1OH substituted at the 5-position fulfills this criterion. We have studied[142] ESPT from 5-(methanesulfonyl)-1-naphthol (5MS1N),[13] whose anion is shown in Scheme 8. Recall, that proton-quenching for 1OH is assumed to occur predominantly at position 5.[25] The sulfonyl substituent protects against such an attack, while promoting the keto resonance shown in the scheme. The keto form is thought to initiate curve-crossing to the GS, leading to the short ES lifetime. Moreover, strong HB donors could stabilize the negative charge on the sulfonyl moiety, hence stabilizing the keto form, decreasing the lifetime even further. Indeed, we find that $1/k_0'$ decreases from 1.85 ns in DMSO to 1.0 ns for EtOH. Commensurate with this change in lifetime, we observed the kinetic transition shown in Figure 21: The R*OH decay is in the A regime for DMSO but switches to the AB regime in EtOH. Thus far, this is the only example of ESPT in the AB regime.

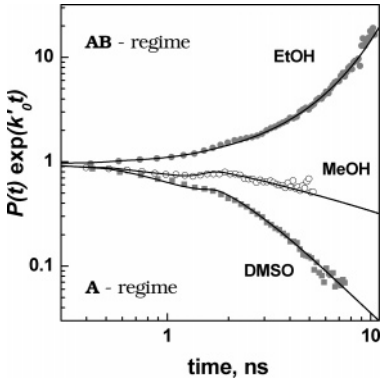

Figure 21. Kinetic transition in ESPT from 5MS1N to various solvents. Points are TCSPC data and lines are fits to the DSE. Adapted from Figure 3 of ref 142, where the various parameters are listed.

E. "A Regime" Asymptotics. Let us now focus in more detail on the "A regime", which is the usual case for exited ROH dyes. The long-time asymptotic behavior (denoted by a $\sim$) can be obtained analytically in this regime,[134]

$$P(t) \sim Z^2 \frac{K_{eq}}{(4\pi Dt)^{3/2}} e^{-k_0' t} \tag{6.13a}$$

$$S(t) \sim Z\left\{1 + \frac{[K_{eq}^q(k_0 - k_0') + k_q e^{-V(a)}]Z}{4\pi D} \frac{1}{\sqrt{\pi Dt}}\right\} e^{-k_0' t} \tag{6.13b}$$

Here two equilibrium coefficients were defined

$$K_{eq} \equiv k_a e^{-V(a)}/k_d \qquad K_{eq}^q \equiv (k_a + k_q)\, e^{-V(a)}/k_d \tag{6.14}$$

(for ESPT, $K_a^* = 1/K_{eq}$) and the ultimate "escape probability", Z, is given by

$$Z \equiv \frac{k_{off}}{k_{off}^q + k_0 - k_0'} \tag{6.15}$$

It is interesting to consider how these general results simplify when either the lifetimes are equal, no quenching occurs, or both:

• **Equal Lifetimes and No Quenching.** In this case[132,143] $Z = 1$, and $S(t)\exp(k_0 t)$ increases monotonically to unity.

• **Equal Lifetimes with Quenching.** In this case $Z = k_{off}/k_{off}^q = k_{-D}/(k_{-D} + k_q)$, namely, the branching ratio between escape and quenching. Equation 6.13b then simplifies to

$$S(t) \sim Z\left(1 + \frac{Zk_q e^{-V(a)}}{4\pi D} \frac{1}{\sqrt{\pi Dt}}\right) e^{-k_0' t} \tag{6.16}$$

This is the asymptotic solution for irreversible geminate association (with a rate constant k_q) starting from $r = a$.[19] Instead of a monotonic increase, there is now a maximum followed by a $t^{-1/2}$ decay to the plateau Z. This result would follow if at long-times the two channels in eqs 6.1 decouple. On the basis of such intuition, Pines & Fleming first proposed this $t^{-1/2}$ decay and verified it experimentally.[144]

• **Different Lifetimes without Quenching.** In this case[133] one can rewrite the survival probability using the more fundamental rate coefficients

$$S(t) \sim \frac{k_d k_D}{Q}\left(1 + \frac{k_a e^{-V(a)}(k_0 - k_0')}{Q}\frac{a_{eff}}{\sqrt{\pi D t}}\right) e^{-k_0' t} \tag{6.17}$$

with $Q \equiv k_d k_D + (k_D + k_a e^{-V(a)})(k_0 - k_0')$. Thus a peak in the lifetime-corrected anion signal is expected even without quenching, provided that the ES lifetime of the anion is longer than that of the acid. The amplitude of the peak is then proportional to $k_a \exp[-V(a)]$.

The "super" photoacid 5CN can transfer its proton to any mixture of water and methanol.[17] As methanol is added into water, lowering ϵ, the proton attraction to the R*O$^-$ increases, whereas its diffusion constant decreases. These are conditions that enhance the quenching reaction. In addition, the lifetime of the anion increases. We used[145] methanol/water mixtures to observe simultaneously the two different power-laws predicted by eqs 6.13.

Figure 22a shows the TCSPC data for 5CN in 11.2 mol % of water in methanol. As the lifetime-corrected acid signal decays, that of the anion rises to a maximum and then decays to the plateau, Z, in eq 6.15. The lines through the data are simultaneous fits to the solution of the DSE. Panel b shows the same data on a log−log scale, after subtracting the constant Z from the lifetime-corrected anion signal. It is seen how the acid tends to the $t^{-3/2}$ law whereas the anion tends to the $t^{-1/2}$ law, with the corresponding asymptotic lines (dash−dot) calculated from eqs 6.13.

F. What Limits the ES Lifetime? Having discussed proton quenching, it is interesting to ask whether other (unimolecular or pseudo-unimolecular) chemical reactions contribute to the nonradiative decay of the excited acid and anion, namely to k_0 and k_0'. The following suggestions have been made, although the relative contribution of each is not well established.

*1. R*OH Decay.* Old 2OH scavenging experiments[146] led to the proposition that H-atoms are formed in the deactivation process of the photoacid in its singlet state

$$R^*OH \rightarrow RO + H \tag{6.18}$$

In the past few years there is renewed interest in this reaction channel. It has been suggested to occur in preference to ESPT for excited phenol in clusters of 2−3 ammonia molecules.[147] High level ab initio calculations revealed an intersection between the $\pi\pi^*$ and $\pi\sigma^*$ states that leads to such radical formation, with possible subsequent disintegration of the hydrogen radical into a proton and a solvated electron.[148] However, the emission from naphthols is red shifted in comparison to phenol, so it is not clear whether the H-atom transfer is an open channel even in their gas-phase clusters.[147] In polar solvents (or with the cyano substituents) the emission is further red-shifted; hence this channel is not likely to be important for most cases considered here.

*2. R*O$^-$ Decay.* Water seems to be particularly efficient in shortening the anion lifetime, and the question arises whether this may be attributed to a specific deactivation reaction. For excited naphtholate, the formation of solvated electrons was suggested[146]

$$R^*O^- \rightarrow RO + e^-_{aq} \tag{6.19a}$$

Lee and Robinson have found a maximum in the lifetime of excited 2-anilinonaphthalene in alcohol/water mixtures.[149] They interpreted this as implying that nonradiative deactivation dominates in pure alcohol solutions, whereas aquated electron formation dominates in pure water. We have observed a similar trend for the ES lifetime of the 5CN anion;[17] see Figure 23. This, then, may support the formation of solvated electorns as a deactivation mechanism for the excited anion in pure water.

An alternative deactivation reaction may be

$$R^*O^- + H_2O \rightarrow ROH + 2OH^- \tag{6.19b}$$

There is plenty of ES energy to promote this channel. The R*O$^-$ excitation energy is typically 2−3 eV, whereas water hydrolysis is endothermic by about 0.6 eV in liquid water, and 1 eV in small water clusters.[150] Water hydrolysis in $(H_2O)_{20}$ clusters was shown by ab initio calculations to be very sensitive to the HB topology, leading for some conformations to spontaneous ion formation.[150] Thus, appropriate HB conformations may promote this deactivation channel also in solution. Photoacids for which eq 6.19b is dominant may be of practical interest, because

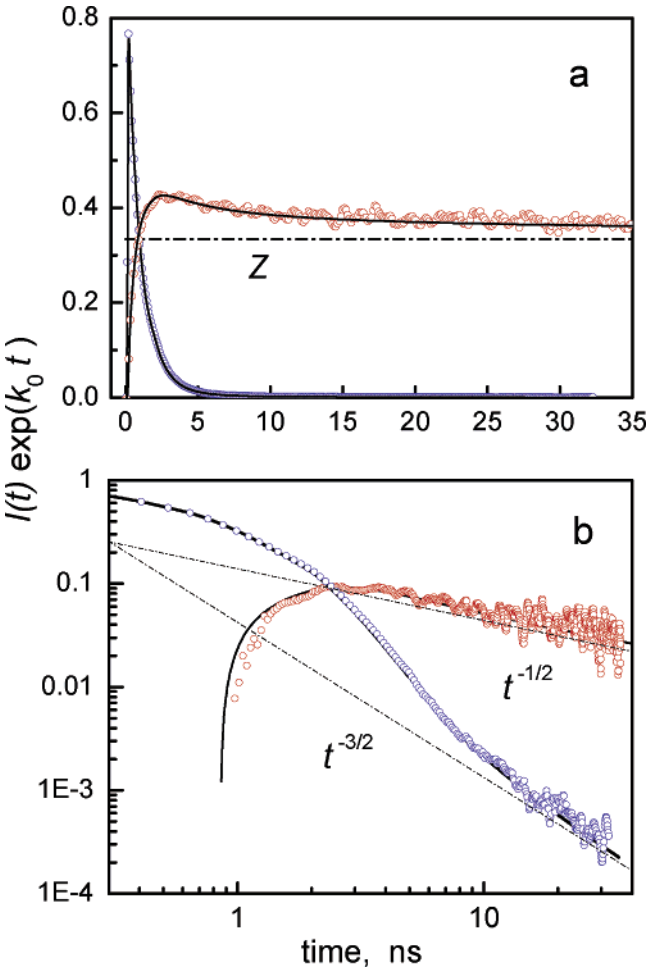

Figure 22. "A regime" kinetics for ESPT to solvent with different lifetimes and quenching. Acid (370 nm, blue circles) and base (570 nm, red circles) fluorescence signals from excited 5CN in 11.2 mol % of methanol are simultaneously fitted to the diffusion model, eqs 6.3 (lines). The dash−dot line in panel (a) is Z from eq 6.15. The dash−dot lines in panel (b) are the two asymptotic power laws from eqs 6.13. Parameters used are $a = 5.5$ Å, $R_D = 16$ Å, $D = 2.2 \times 10^{-5}$ cm^2/s, $k_d = 1.9$ ns^{-1}, $k_a/(4\pi a^2) = 15.2$ Å/ns, $k_q/(4\pi a^2) = 12$ Å/ns, $1/k_0 = 5.7$ ns, and $1/k_0 = 11.3$ ns. Adapted from Figures 2 and 3 of ref 145.

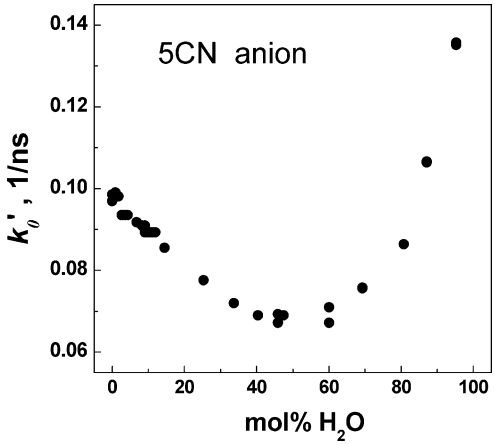

Figure 23. Dependence of the ES decay rate coefficient of the 5CN anion on solvent composition in methanol/water mixtures. Adapted from Figure 14 of ref 17.

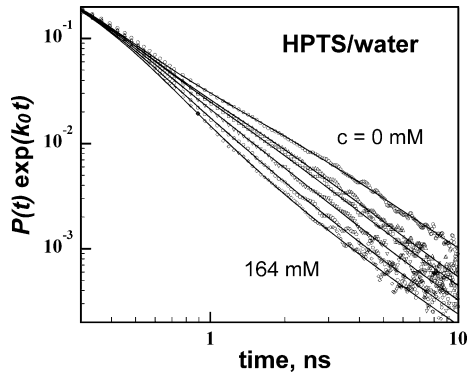

Figure 24. Salt effect on the transient fluorescence from HPTS (at the R*OH frequency, 435 nm) for aqueous solutions of varying $NaNO_3$ concentrations (top to bottom: $c = 0$, 12, 24, 47, 85, and 164 mM). Lines are fits to the diffusion model, with DH screening, adjusted D and the remaining parameters kept constant: $a = 6$ Å, $R_D = 28.3$ Å, $k_d = 7.1$ ns^{-1}, $k_a/(4\pi a^2) = 5$ Å/ns, $1/k_0 = 5.3$ ns, $1/k_0' = 5.4$ ns. Adapted from Figure 2 of ref 151.

following light absorption they eject a proton on a short time scale and a hydroxide at longer times.

VII. Salt Effects

Thus far we have focused on the individual kinetic steps for a single excited photoacid. The problem is made more complex by the addition of salts. We consider here only salts of strong electrolytes, which are fully dissociated into ions. These may be divided into two classes: salts of stronger and weaker acids.

Salts of strong acids are inert, because their anion is a weak base that does not react readily with the proton. At low concentrations, such salts only modify the long-range potential, by screening the Coulomb interaction between H^+ and R^*O^-. Salts of weaker acids dissociate to give a stronger ionic base, B^-. It may react with the proton, either before or after R*OH dissociation. The present section extends the fundamental diffusion model to these two cases. The success of the extended model lends further support to our basic interpretation of the kinetics as a reversible geminate diffusion-influenced reaction.

A. Inert Salts. Figure 24 shows the effect of an inert salt ($NaNO_3$) on the photodissociation kinetics of HPTS in water.[151] HPTS is a convenient probe to use, because it exhibits similar acid and base lifetimes and little proton quenching. The log−log scale emphasizes the long-time $t^{-3/2}$ decay due to reversible geminate recombination. With increasing salt concentration, its amplitude decreases, and this is attributed to screening of the Coulomb attraction between the dissociated proton and the 4-times charged HPTS anion.

Within the framework of the diffusion model in section VIA, one solves the DSE in eq 6.3a after replacing the Coulomb potential of eq 6.2 by the Debye−Hückel (DH) screened potential

$$V(r) = -\frac{R_D}{r}\frac{\exp[-\kappa(r-a)]}{1+\kappa a} \qquad \kappa^2 \equiv \frac{8\pi e^2 c}{k_B T \epsilon} \quad (7.1)$$

Here $1/\kappa$ is the radius of the "ionic atmosphere" for a univalent salt of concentration c.[98] The same a is used in the electrostatic and the diffusion problems. Inserting parameters, $\kappa a = 1.97\sqrt{c}$ with c in molar, producing a concentration dependence in the interaction potential.

With all parameters kept at their respective values for pure water and only κ varying with c, the attenuation of the long-time tail is too strong. However, according to the Kohlraush law (treated theoretically by Onsager),[98] D decreases with increasing c following a $\sqrt{c}$ dependence. This should enhance geminate recombination and partly compensate for the increase in screening. Thus, to obtain the fits in Figure 24, D was adjusted at each concentration. It was indeed found to decrease, from 9.3×10^{-5} cm^2/s in pure water to 7.0×10^{-5} cm^2/s at 164 mM salt,[151] following the $\sqrt{c}$ law (albeit with an excessive slope).

B. Salts of Weak Acids. Salts of weak acids are not inert, because their anion, B^-, is a base that can bind a proton. Common examples are fluoride, F^-, and acetate, $CH_3CO_2^-$. Their pK_a values lie between the GS and ES acidity constants of the photoacid under consideration, so that they do not react with it in the GS but do so in its ES.

Three (irreversible) reactive channels are now possible for the B^-:

- Scavenge the dissociated proton from solution

$$B^- + H^+ \xrightarrow{k_s} BH \quad (7.2a)$$

- Diffuse to pick up the proton from the excited R*OH

$$B^- + R^*OH \xrightarrow{k_{PT}} BH + R^*O^- \quad (7.2b)$$

- Form a HB complex already in the GS

$$ROH\cdots B^- + h\nu \rightarrow R^*OH\cdots B^- \rightarrow BH + R^*O^- \quad (7.2c)$$

The first reaction dominates at low B^- concentrations, the second at intermediate concentrations and the last at very large [B^-]. Weller apparently considered only the second reaction when discussing the acetate effect on the 2OH fluorescence spectrum.[2,152] The reaction in eq 7.2c behaves like intramolecular PT;[66,79] see section IVB. Thus we analyze below the diffusion-influenced kinetics prevailing in the first two cases.[153−157]

1. Proton Scavenging. Proton scavenging in eq 7.2a is dominant for low salt concentrations, typically 1−20 mM. In this case the photoacid dissociates before a direct collision with the scavenger takes place. Goldberg et al. measured the excited HPTS kinetics in aqueous solutions with varying acetate concentrations in this range.[153] As noted above, HPTS is a "nice" photoacid for performing such experiments, because $k_0 \approx k_0'$ and $k_q \approx 0$.

To explain the acetate effect, a $-ck_s\,p(r,t)$ term was added to the DSE in eq 6.3a, where k_s is the bimolecular scavenging rate coefficient in eq 7.2a and $c = [B^-]$. This is equivalent to modifying the ES decay rate, replacing k_0' by $k_0' + ck_s$. On this

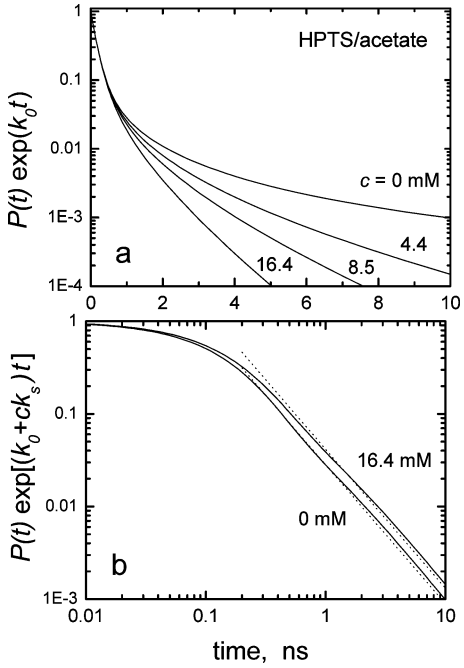

Figure 25. Scavenger effect on photoacid dissociation. Lines are best-fits to TCSPC data (not shown) of HPTS (acid form) in aqueous solutions containing various CH_3COO^- concentrations (indicated):[153] (a) semilog scale; (b) multiplied additionally by $\exp(ck_s t)$ and displayed on a log−log scale. Dotted lines show asymptotics from eqs 6.13a and 7.3. Parameters taken from Table 1 of ref 153: $a = 7$ Å, $R_D = 28.4$ Å, $k_d = 7.5$ ns^{-1}, $k_a/(4\pi a^2) = 7.5$ Å/ns, $1/k_0 = 1/k_0' = 5.3$ ns, $k_s = 4.5 \times 10^{10}$ M^{-1} s^{-1}, $D = 9.3 \times 10^{-5}$ cm^2/s.

mean-field level, the many scavenger molecules are represented by a uniform and constant concentration c. For simplicity, the effect of varying ionic strength with c was not taken here into account. The justification for this is not only that c is small (up to 16.4 mM), but also that screening of the H^+/B^- interaction has an opposite effect on the recombination probability than the screening of the H^+/R^*O^- interaction.

The mean-field DSE was shown to produce a good description of the measured scavenging effect, although an effective c was used that differs from its true value by about 10%.[153] The best-fit theoretical curves are shown in Figure 25a. The long-time $t^{-3/2}$ tail, which is due to geminate recombination, is strongly attenuated by the added scavenger and switches into an asymptotic exponential decay.

At the time, the solution to the DSE with scavenging was not known, because it is isomorphic with the two-lifetime problem. Having worked out the theory in sections VIC−E, all that is needed is to replace k_0' by $k_0' + ck_s$ in all of our equations. Thus, in the usual A regime, $P(t)\exp[(k_0' + ck_s)t]$ should decay asymptotically according to the $t^{-3/2}$ law in eq 6.13a. For HPTS the prefactor in eq 6.15 simplifies to

$$Z = k_{off}/(k_{off} - ck_s) \tag{7.3}$$

Hence unlike the case of quenching, when Z decreases with increasing k_q, here it *increases* with increasing ck_s. This behavior is demonstrated in Figure 25b. Moreover, the kinetics should undergo a transition when $ck_s = k_{off}$.

These predictions have not yet been checked experimentally. They require more accurate data and will hold only if this mean-field description of scavenging is valid over a wide dynamic range.

2. Direct Acid−Base Reaction. The ES bimolecular reaction in eq 7.2b dominates at higher base concentrations (1−4 M),

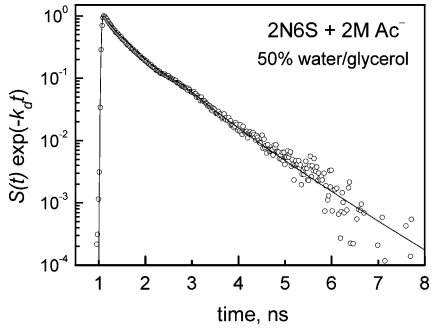

Figure 26. Direct bimolecular acid−base reaction between a 2N6S photoacid and 2 M acetate anion in an aqueous solution containing 50 vol % glycerol. Circles are the experimental data, multiplied by $\exp(k_0 t)$. The line is an IRF-convoluted fit to the Smoluchowski theory in eq 7.6. Parameters used in the fit are $a = 7$ Å, $\epsilon = 61$, $R_D = 9.1$ Å, $1/k_0 = 1/k_0' = 10$ ns, $k_{PT} = 9.4 \times 10^9$ M^{-1} s^{-1}, $D = 0.067 \times 10^{-5}$ cm^2/s, and $1/k_d = 12$ ns. Extracted from Figure 6 of ref 156.

when the initial acid−base distances are sufficiently small to be covered by diffusion before the proton dissociates. This reaction has been studied in the time domain in several recent publications.[154−157] Figure 26 shows the ES kinetics of 2-hydroxynaphthalene-6-sulfonate (2N6S) with 2 M acetate in an aqueous solution containing 50% (by volume) of glycerol.[156] The added glycerol slows down the relative acid−base diffusion and thus enhances the diffusional effects. The lifetime-corrected fluorescence signal (circles) decays initially fast but then slows down to a near-exponential decay.

The simplest approach for treating these data[155,156] is via the Smoluchowski theory[158] of pseudo-unimolecular ($c \equiv [B^-] \gg [R^*OH]$) irreversible diffusion-influenced reactions, which is the most fundamental many-body theory in the field of diffusion-influenced reactions.[19] In the limit that the R*OH is static (and only the B^- diffuse), it is exact[159,160] yet provides an excellent approximation also when the acid moves.[161]

In this approach, one first solves a DSE for a *geminate* GS acid−base pair with a relative diffusion constant D. This is simpler than eq 6.3a, because we set $k_d = k_q = k_0 = 0$ and replace k_a by the PT rate constant k_{PT}:

$$\frac{\partial}{\partial t}p(r,t) = \left[r^{-2}\frac{\partial}{\partial r}Dr^2 e^{-V(r)}\frac{\partial}{\partial r}e^{V(r)} - k_{PT}\frac{\delta(r-a)}{4\pi a^2}\right]p(r,t) \tag{7.4}$$

whereas $\partial P(t)/\partial t = k_{PT}\, p(a,t)$. The initial condition is an equilibrium distribution of the B^- around a central R*OH molecule

$$p(r,0) = \exp[-V(r)] \tag{7.5}$$

whereas $P(0) = 0$. The survival probability, $S(t)$, of the unreacted acid for our irreversible *many-body* problem is connected with the solution of eq 7.4 as follows:[159,160]

$$S(t) = \exp[-cP(t)] = \exp[-c\int_0^t k(t')\,dt'] \tag{7.6}$$

where $k(t) \equiv k_{PT}p(a,t)$ is the celebrated "time-dependent rate coefficient".[162]

In the absence of an interaction potential, eq 7.4 can be solved analytically for $p(r,t)$, from which one finds[19]

$$k(t) = \frac{k_D\, k_{PT}}{k_D + k_{PT}}\left[1 + \frac{k_{PT}}{k_D}\phi(t;\sigma)\right] \tag{7.7}$$

Here $\phi(t;\sigma)$ is the function defined in eq 6.11, $a\sigma = 1 + k_{PT}/k_D$

and $k_D = 4\pi Da$. Thus $k(t)$ starts from the large value, k_{PT}, and decays to its asymptotic value, $k_D k_{PT}/(k_D + k_{PT})$. Consequently, $S(t)$ decays initially faster than exponential, becoming exponential at long times.

In the presence of a potential, two useful approximations were suggested.[160] Alternately, the exact $k(t)$ can be obtained using the SSDP software.[139] Here we use the DH potential in eq 7.1, with $\kappa = 2.9\sqrt{c/\epsilon}$ Å^{-1} (c in molar). Although it is not quite adequate for such a high electrolyte concentration, the screening is so strong ($1/\kappa \approx 2$ Å for $c = 2$ M) that one may almost eliminate the potential altogether. To account for the competing channel in eq 7.2a, we multiply $S(t)$ from eq 7.6 by $\exp(-k_d t)$, using a k_d that was measured separately in the same solvent without acetate. For simplicity, geminate proton recombination is neglected. Figure 26 compares this theory (line) with the lifetime corrected TCSPC signal of R*OH. An extended comparison for a whole series of glycerol compositions is given elsewhere.[155,156]

The agreement with the Smoluchowski theory is good. For many years this theory was utilized mainly for fluorescence quenching,[163,164] but unfortunately the initial nonexponential phase was not conspicuous.[165] Nowadays, direct ES acid−base reactions provide some of the best available examples for the applicability of the theory.

VIII. pH Effect as a Many-Body Problem

The pH effect on ESPT to solvent formed the basis for the fluorimetric titration method utilized by Weller to determine pK_a^* values.[2] The basic assumption is that pseudo-equilibrium is reached in the reversible ES reaction, as suggested by eq 1.1. When time-resolved measurements became feasible,[127,166] the data were typically fitted to the biexponential kinetics predicted from chemical rate equations.[167] In view of the nonexponential kinetics observed for the geminate pair (see above), Huppert et al.[168] raised the question whether the homogeneous reaction between R^*O^- and a concentration, c, of protons is truly (multi)-exponential. This, in turn, motivated the development of the many-body theory of reversible diffusion-influenced reactions, which is described below together with some experimental verification.[169,170]

A. Theoretical Model. The theoretical model is the simplest possible *many-body* extension of the diffusion model in section VIA for the reversible C ⇌ A + B reaction. We consider only the GS problem in detail. It applies also to the ES if $k_0 = k_0'$. In this model, a static C molecule is located at the origin (the "target problem"). It is a sphere of radius a, surrounded by a concentration c of identical point particles, B. The B particles diffuse with a diffusion constant D and interact only with C, or only with A, via the same spherically symmetric potential, $V(r)$ (in units of $k_B T$). Ascribing the mobility only to the B's is a rather good approximation when dealing with protons.

C may dissociate with a rate constant k_d to form an A−B pair at contact, and then the geminate B competes with all other B's for rebinding. When A and B collide they react to form C with a rate constant k_a. However, if C collides with B nothing happens (a reflecting boundary condition then applies). As for the geminate problem, no angular dependence is assumed for the chemical reactivity, so that the spherical symmetry of the problem is maintained.

Unlike the discussion of salt effects, when a mean-field approach was applied, one is interested in developing a truly many-particle treatment to this problem. This means that each B_i is treated microscopically, its position being defined by its distance r_i from A or from C. The exact problem then involves the joint probability density for r_1, r_2, ..., so that for N particles an N-dimensional diffusion equation needs to be solved for the A + B state. This, in turn, is coupled to N other diffusion equations depicting a given B_i, which is bound to A to form C. Eventually, one takes the thermodynamic limit when both N and the volume tend to infinity while maintaining their ratio, c, constant.

Clearly, this is a formidable problem. One may hope to find an exact solution only by simulations. An accurate Brownian dynamics methodology was developed by Edelstein and Agmon,[171] first in one dimension and subsequently extended to three dimensions.[172−174] The principles and "tricks" utilized to perform these simulations, over a wide time range and for many B particles, can be found in the original publications. Although the simulations are currently limited to static A or C and no interaction potential, their availability enabled one to test the various theories, and eventually converge onto the most promising analytical theory described below. This also motivated a renewed comparison with experiment.

B. Analytical Results. Of the many analytical approximations suggested for the many body C ⇌ A + B reaction (see ref 173 for an overview), the most accurate description of the GS reaction is given by the multi-particle kernel 1 (MPK1) theory of Sung and Lee.[175] This solution applies also to the ES reaction when the ES lifetimes are equal. A convenient starting point is a convolution relation for the probability, $P(t)$, of observing the bound state C:

$$dP(t)/dt = ck_a e^{-V(a)} \int_0^t \Sigma(t-\tau)[1 - P(\tau)]\, d\tau - k_d \int_0^t \Sigma(t-\tau) P(\tau)\, d\tau \quad (8.1)$$

The rate kernel, $\Sigma(t)$, contains memory effects due to the reversibility of the reaction and the effect of diffusion. Ordinary chemical kinetics apply when it is a delta function, $\Sigma(t) = \delta(t)$. The points to note are that the *same* rate kernel appears for both recombination and dissociation terms and that this relation is formally exact, although the exact $\Sigma(t)$ is, of course, unknown.

As usual, one takes the Laplace transform, defining $F(s)^{-1} \equiv \hat{\Sigma}(s) = \int_0^\infty \Sigma(t) \exp(st)\, dt$. The function $F(s)$ is sometimes called the "diffusion factor function", as it factors out the effect of diffusion on the kinetics. Starting from the bound state, $P(0) = 1$, the Laplace transformed eq 8.1 becomes

$$\hat{P}(s) = \frac{1}{s} \frac{cK_{eq} + (s/k_d)F(s)}{1 + cK_{eq} + (s/k_d)F(s)} \quad (8.2)$$

with K_{eq} from eq 6.14. In the chemical kinetic limit of fast diffusion $F(s) = 1$. Various approximate theories imply different approximations for $F(s)$.[173] However, for asymptotically long times ($s \to 0$) the terms containing $F(s)$ cancel altogether, and one gets

$$P(\infty) = cK_{eq}/(1 + cK_{eq}) \quad (8.3)$$

Only in this limit is the chemical kinetic result of general validity.

The most successful form of $F(s)$, that of the MPK1 approximation,[175] is a linear combination of two factor functions

$$F(s) \approx \frac{1}{1 + cK_{eq}} F_{gem}(s) + \frac{cK_{eq}}{1 + cK_{eq}} F_{irr}(s) \quad (8.4)$$

for the geminate and irreversible problems, $F_{gem}(s)$ and $F_{irr}(s)$, respectively. The irreversible solution is given by the Smolu-

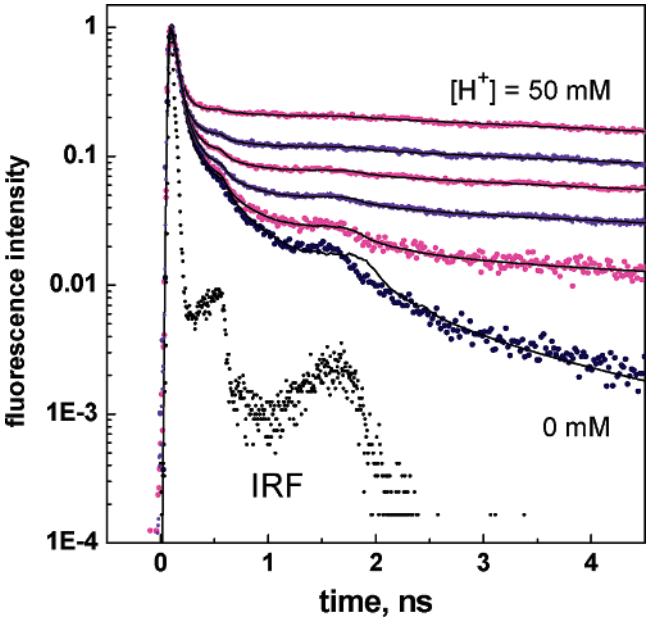

Figure 27. Time dependence of 2N68DS fluorescence in aqueous solutions of varying proton concentrations, top to bottom: 50, 20, 10, 5, 2.5, and 0 mM HCl. Lines are IRF-convoluted multiexponential fits used to prepare Figure 28. Adapted from Figure 3 of ref 169.

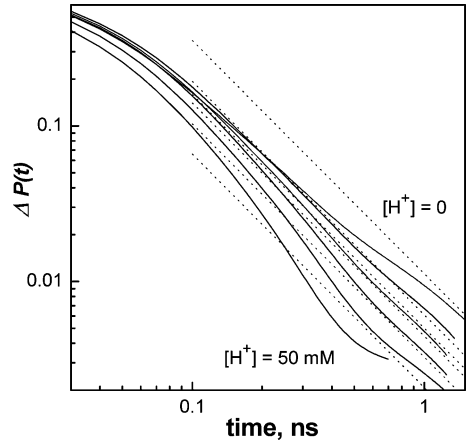

Figure 28. Approach to (quasi) equilibrium in ESPT from 2N68DS to aqueous solutions containing various HCl concentrations (top to bottom: 0, 2.5, 5, 10, 20 and 50 mM). Lines were extracted from multiexponential fits to the data in Figure 27. Dashed lines were calculated from eq 8.5, using a concentration-dependent K_{eq} calculated from $P(\infty)$ in eq 8.3. Adapted from Figure 7 in ref 169.

chowski result in eq 7.6, only with an *effective* concentration, $c_{eff} = c + K_{eq}^{-1}$, replacing the c there. The exact form for these two factor functions can be found elsewhere.[173,175] When eq 8.4 is inserted into eq 8.2 and the Laplace transform is inverted, the results are almost indistinguishable from those of three-dimensional Brownian simulations of the target problem (without a potential).

The long-time asymptotic behavior of the MPK1 expression can be obtained analytically

$$\Delta P(t) \equiv P(t) - P(\infty) \sim \frac{K_{eq}}{(1 + cK_{eq})^3 (4\pi Dt)^{3/2}} + \ldots \quad (8.5)$$

It has first been derived from other approximations[176,177] and subsequently shown to be exact.[178,179] The approach to the limiting plateau in eq 8.3 is thus a power law, and not exponential, as might be expected from chemical kinetics. The effect of diffusion is indeed difficult to obliterate. It results from the many cycles of dissociation and recombination. Each sequential dissociation event produces one B particle at contact with A, but the remaining B's have meanwhile progressed closer to equilibrium. Eventually, the problem approaches the situation of an A−B pair at contact, immersed in an equilibrium distribution of B's. This limit then becomes a "dressed"geminate problem, retaining the characteristic $t^{-3/2}$ behavior, albeit with concentration-dependent coefficients.

For *different* lifetimes, the whole problem has to be reconsidered. Simulations for the ES problem with different lifetimes have recently been reported.[174,180] The best overall agreement with these data is obtained by the "unified Smoluchowski approximation" (USA) of Szabo and co-workers.[181] In this theory, the diffusion factor function becomes a linear combination of two irreversible Smoluchowski-like terms with effective concentrations. Unfortunately, its long-time behavior could not be obtained analytically.

C. Comparison with Experiment. Figure 27 shows the effect of adding increasing amounts of HCl to an aqueous solution of 2N68DS, on its transient fluorescence signal.[169] Though theory assumes equal ES lifetimes, 2N68DS has somewhat different lifetimes, 9.2 and 12.4 ns for the acid and base, respectively. This makes the comparison less than quantitative. As seen in the figure, the lower the pH the larger the quasi-equilibrium plateau approached by the lifetime-corrected R*OH fluorescence. This again confirms the occurrence of adiabatic proton recombination with the excited anion.

The limiting plateau agrees semiquantitatively with $P(\infty)$ from eq 8.3, increasing with proton concentration, c. This increase is not as fast as might be expected because of increasing ionic screening by the added HCl, which reduces K_{eq}. The dependence of K_{eq} on c could be explained by the DH potential in eq 7.1, except that a value of $B = 0.46$ M$^{-1/2}$ was used in $\kappa = Bc^{1/2}$ instead of the theoretical value of 0.33 M$^{-1/2}$.

To extract the approach to the quasi-equilibrium state, the data were fitted to a multiexponential function that was convoluted with the IRF. The fitted function was multiplied by $\exp(k_0' t)$ and the constant $P(\infty)$ subtracted from it. The results are shown in Figure 28, and they indeed appear to follow the $t^{-3/2}$ behavior in eq 8.5. In a parallel measurement on HPTS (for which the assumption $k_0 \approx k_0'$ is much better), Pines and Pines[170] were even able to verify that the power on the $1 + cK_{eq}$ term in the denominator is indeed 3 (and not 2, as previously believed).

IX. Conclusion

A combination of experiment, theory, and simulations unravels the elementary steps involved in the phenomenon of photoacidity of ROH-type photoacids. These steps begin with the atosecond intramolecular charge rearrangement, revealed by quantum chemistry calculations and solvatochromic shifts. Electronic charge flows from the OH group to the aromatic ring system, more strongly so in the anion than the acid. This induces a femtosecond HB rearrangement, strengthening the HB donated from the OH to the solvent, in preparation of the transfer step. The PT step itself, which occurs in picoseconds, appears to depend crucially on the solvent. This is manifested in unusual dependence of the dissociation rate parameter on water concentration and temperature. The dissociated proton diffuses in aqueous solutions anomalously fast, each proton hop taking place in just 1−2 ps. New simulation results point toward a

collective participation of HBs in the Grotthuss mechanism of proton mobility.

The dissociated proton continues to engage the excited anionic base in recombination or quenching reactions. These fast processes (on the 100 ps to 100 ns time scale) are necessarily diffusion-influenced. A diffusion model was thus developed that describes ES reversible geminate recombination, with different ES lifetimes for acid and base, and with quenching. This model reveals an interesting kinetic transition. In the more common "A regime", it exhibits different long-time power-law kinetics for acid and base. These effects were verified experimentally. On the nanosecond time scale, the ES decays to the GS, and possible nonradiative decay mechanisms were discussed. The diffusional kinetics is compounded when salts or acids are added to the solution. This introduces effects of ionic screening, proton scavenging by basic anions, and many-body competition for rebinding between the geminate and homogeneous protons. These were treated theoretically and compared with experimental data. This motivated the development of a new theoretical subfield of diffusion-influenced reactions dealing with *reversible* reactions.

This does not yet complete the saga of the excited photoacid, which may get involved in additional processes at even longer times. For example, it may undergo intersystem crossing into the triplet state. The RO^- eventually rebinds the proton on the nanosecond to microsecond time scale once back in the GS,[182−184] completing the cycle in Scheme 2. The present exposition did not address all possible extensions and applications of the ESPT phenomenon: It only touched the growing field of ESPT in gas-phase clusters.[10,39−45,147] It did not discuss ESPT in bifunctional compounds,[185] which may have an important role in analytical chemistry of metals.[186] ESPT can also occur in micelles, reverse micelles,[187−189] and other supramolecular assemblies.[190] It serves as a useful probe of membranes, channels, and proteins.[191,192] It also occurs naturally in some proteins, such as the green fluorescent protein.[193,194]

Given the increasing number of applications of *intermolecular* ESPT reactions, it is hoped that the present exposition of the fundamental steps involved in the cascade of processes triggered by light excitation of ROH photoacids will be of use in future studies.

Acknowledgment. I thank my students and collaborators for participating in the studies described herein: Boiko Cohen, Irina V. Gopich, Dan Huppert, Hadas Lapid, Kyril M. Solntsev, Ehud Pines, Alexander V. Popov, Wolfgang Rettig, Attila Szabo, Laren M. Tolbert, and Gregory A. Voth. This research was supported in part by the Israel Science Foundation (grant number 191/03). The Fritz Haber Research Center is supported by the Minerva Gesellschaft für die Forschung, GmbH, München, FRG.

References and Notes

(1) Förster, T. *Z. Elektrochem.* **1950**, *54*, 531.
(2) Weller, A. *Prog. React. Kinet.* **1961**, *1*, 187.
(3) Förster, T. *Pure Appl. Chem.* **1970**, *24*, 443.
(4) Ireland, J. F.; Wyatt, P. A. H. *Adv. Phys. Org. Chem.* **1976**, *12*, 131.
(5) Shizuka, H. *Acc. Chem. Res.* **1985**, *18*, 141.
(6) Gutman, M.; Nachliel, E. *Biochim. Biophys. Acta* **1990**, *1015*, 391.
(7) Arnaut, L. G.; Formosinho, S. J. *J. Photochem. Photobiol. A* **1993**, *75*, 1.
(8) Tolbert, L. M.; Solntsev, K. M. *Acc. Chem. Res.* **2002**, *35*, 19.
(9) Formosinho, S. J.; Arnaut, L. G. *J. Photochem. Photobiol. A* **1993**, *75*, 21.
(10) Douhal, A.; Lahmani, F.; Zewail, A. H. *Chem. Phys. Lett.* **1996**, *207*, 477.
(11) Soumillion, J. P.; Vandereecken, P.; Van Der Auweraer, M.; De Schryver, F. C.; Schanck, A. *J. Am. Chem. Soc.* **1989**, *111*, 2217.
(12) Tolbert, L. M.; Haubrich, J. E. *J. Am. Chem. Soc.* **1990**, *112*, 8163.
(13) Tolbert, L. M.; Haubrich, J. E. *J. Am. Chem. Soc.* **1994**, *116*, 10593.
(14) Huppert, D.; Tolbert, L. M.; Linares-Samaniego, S. *J. Phys. Chem. A* **1997**, *101*, 4602.
(15) Solntsev, K. M.; Huppert, D.; Tolbert, L. M.; Agmon, N. *J. Am. Chem. Soc.* **1998**, *120*, 7981.
(16) Solntsev, K. M.; Huppert, D.; Agmon, N. *J. Phys. Chem. A* **1999**, *103*, 6984.
(17) Solntsev, K. M.; Huppert, D.; Agmon, N.; Tolbert, L. M. *J. Phys. Chem. A* **2000**, *104*, 4658.
(18) Clower, C.; Solntsev, K. M.; Kowalik, J.; Tolbert, L. M.; Huppert, D. *J. Phys. Chem. A* **2002**, *106*, 3114.
(19) Rice, S. A. *Diffusion-Limited Reactions*; Comput. Chem. Kinet.; Elsevier: Amsterdam 1985; Vol. 25.
(20) Weller, A. *Z. Elektrochem.* **1952**, *56*, 662.
(21) Jackson, G.; Porter, G. *Proc. R. Soc. London A* **1961**, *260*, 13.
(22) Baba, H.; Suzuki, S. *J. Chem. Phys.* **1961**, *35*, 1118.
(23) Schulman, S. G. *Spectrosc. Lett.* **1973**, *6*, 197.
(24) Tobita, S.; Shizuka, H. *Chem. Phys. Lett.* **1980**, *75*, 140.
(25) Webb, S. P.; Philips, L. A.; Yeh, S. W.; Tolbert, L. M.; Clark, J. H. *J. Phys. Chem.* **1986**, *90*, 5154.
(26) Granucci, G.; Hynes, J. T.; Millié, P.; Tran-Thi, T.-H. *J. Am. Chem. Soc.* **2000**, *122*, 12243.
(27) Solntsev, K. M.; Huppert, D.; Agmon, N. *J. Phys. Chem. A* **1998**, *102*, 9599.
(28) Dewar, M. J. S.; Stewart, J. J. P.; Ruiz, J. M.; Liotard, D.; Healy, E. F.; Dennington, R. D., II. In *AMPAC Version 6.55*. Semichem., Shawnee 1997−1999.
(29) Agmon, N.; Rettig, W.; Groth, C. *J. Am. Chem. Soc.* **2002**, *124*, 1089.
(30) Minkin, V. I.; Osipov, O. A.; Zhdanov, Y. A. *Dipole Moments in Organic Chemistry*; Plenum: New York 1970.
(31) Wiberg, K. B. *Chem. Rev.* **2001**, *101*, 1317.
(32) Zilberg, S.; Haas, Y. *J. Phys. Chem. A* **1998**, *102*, 10843.
(33) Horng, M. L.; Gardecki, J. A.; Papazyan, A.; Maroncelli, M. *J. Phys. Chem.* **1995**, *99*, 17311.
(34) Kamlet, M. J.; Abboud, J.-L. M.; Abraham, M. H.; Taft, R. W. *J. Org. Chem.* **1983**, *48*, 2877.
(35) Laurence, C.; Nicolet, P.; Dalati, M. T.; Abboud, J.-L. M.; Notario, R. *J. Phys. Chem.* **1994**, *98*, 5807.
(36) In an excitation spectrum one measures fluorescence at a fixed frequency as a function of the excitation wavelength. The outcome is similar to an absorption spectrum.
(37) Tran-Thi, T.-H.; Prayer, C.; Millié, P.; Uznanski, P.; Hynes, J. T. *J. Phys. Chem. A* **2002**, *106*, 2244.
(38) Fang, W.-H. *J. Chem. Phys.* **2000**, *112*, 1204.
(39) Plusquellic, D. F.; Tan, X.-Q.; Pratt, D. W. *J. Chem. Phys.* **1992**, *96*, 8026.
(40) Humphrey, S. J.; Pratt, D. W. *J. Chem. Phys.* **1996**, *104*, 8332.
(41) Henseler, D.; Tanner, C.; Frey, H.-M.; Leutwyler, S. *J. Chem. Phys.* **2001**, *115*, 4055.
(42) Humphrey, S. J.; Pratt, D. W. *J. Chem. Phys.* **1997**, *106*, 908.
(43) Bach, A.; Leutwyler, S. *J. Chem. Phys.* **2000**, *112*, 560.
(44) Coussan, S.; Bach, A.; Leutwyler, S. *J. Phys. Chem. A* **2000**, *104*, 9864.
(45) Bach, A.; Coussan, S.; Müller, A.; Leutwyler, S. *J. Chem. Phys.* **2000**, *113*, 9032.
(46) Smulevich, G.; Foggi, P. *J. Chem. Phys.* **1987**, *87*, 5657.
(47) Marzocchi, M. P.; Mantini, A. R.; Casu, M.; Smulevich, G. *J. Chem. Phys.* **1998**, *108*, 534.
(48) Chudoba, C.; Nibbering, E. T. J.; Elsaesser, T. *Phys. Rev. Lett.* **1998**, *81*, 3010.
(49) Nibbering, E. T. J.; Chudoba, C.; Elsaesser, T. *Isr. J. Chem.* **1999**, *39*, 333.
(50) Oikawa, A.; Abe, H.; Mikami, N.; Ito, M. *J. Phys. Chem.* **1984**, *88*, 5180.
(51) Johnson, J. R.; Jordan, K. D.; Plusquellic, D. F.; Pratt, D. W. *J. Chem. Phys.* **1990**, *93*, 2258.
(52) Knochenmuss, R.; Solntsev, K. M.; Tolbert, L. M. *J. Phys. Chem. A* **2001**, *105*, 6393.
(53) Brønsted, J. N.; Pedersen, K. *Z. Phys. Chem.* **1924**, *108*, 185.
(54) Brønsted, J. N. *Chem. Rev.* **1928**, *5*, 231.
(55) Marcus, R. A. *J. Phys. Chem.* **1968**, *72*, 891.
(56) Marcus, R. A. *Faraday Symp. Chem. Soc.* **1975**, *10*, 60.
(57) Johnston, H. S. *Gas-Phase Reaction Rate Theory*; Ronald Press: New York 1960.
(58) Agmon, N.; Levine, R. D. *Chem. Phys. Lett.* **1977**, *52*, 197.
(59) Agmon, N.; Levine, R. D. *Isr. J. Chem.* **1980**, *19*, 330.
(60) Agmon, N. *Int. J. Chem. Kinet.* **1981**, *13*, 333.

(61) Pauling, L. *J. Am. Chem. Soc.* **1947**, *69*, 542.
(62) Andrieux, C. P.; Gamby, J.; Hapiot, P.; Savéant, J.-M. *J. Am. Chem. Soc.* **2003**, *125*, 10119.
(63) Peters, K. S.; Kim, G. *J. Phys. Chem. A* **2004**, *108*, 2598.
(64) Peters, K. S.; Cashin, A.; Timbers, P. *J. Am. Chem. Soc.* **2000**, *122*, 107.
(65) Pines, E.; Fleming, G. R. *J. Phys. Chem.* **1991**, *95*, 10448.
(66) Pines, E.; Magnes, B.-Z.; Lang, M. J.; Fleming, G. R. *Chem. Phys. Lett.* **1997**, *281*, 413.
(67) Pines, E.; Pines, D.; Barak, T.; Magnes, B.-Z.; Tolbert, L. M.; Haubrich, J. E. *Ber. Bunsen-Ges. Phys. Chem.* **1998**, *102*, 511.
(68) Barroso, M.; Arnaut, L. G.; Formosinho, S. J. *J. Photochem. Photobiol. A* **2002**, *154*, 13.
(69) Kiefer, P. M.; Hynes, J. T. *J. Phys. Chem. A* **2002**, *106*, 1834.
(70) Kiefer, P. M.; Hynes, J. T. *J. Phys. Chem. A* **2002**, *106*, 1850.
(71) Schwartz, B. J.; Peteanu, L. A.; Harris, C. B. *J. Phys. Chem.* **1992**, *96*, 3591.
(72) Arthen-Engeland, T.; Bultmann, T.; Ernsting, N. P.; Rodriguez, M. A.; Thiel, W. *Chem. Phys.* **1992**, *163*, 43.
(73) Chudoba, C.; Riedle, E.; Pfeiffer, M.; Elsaesser, T. *Chem. Phys. Lett.* **1996**, *263*, 622.
(74) Arzhantsev, S. Y.; Takeuchi, S.; Tahara, T. *Chem. Phys. Lett.* **2000**, *330*, 83.
(75) Trakhtenberg, L. I.; Klochikhin, V. L.; Pshezhetsky, S. Y. *Chem. Phys.* **1982**, *69*, 121.
(76) Trakhtenberg, L. I.; Klochikhin, V. L. *Chem. Phys.* **1998**, *232*, 175.
(77) Borgis, D.; Hynes, J. T. *J. Phys. Chem.* **1996**, *100*, 1118.
(78) Lee, S.; Hynes, J. T. *J. Chim. Phys.-Phys. Chim. Biol.* **1996**, *93*, 1783.
(79) Rini, M.; Magnes, B.-Z.; Pines, E.; Nibbering, E. T. J. *Science* **2003**, *301*, 349.
(80) Agmon, N. *Chem. Phys. Lett.* **1995**, *244*, 456.
(81) Agmon, N. *J. Chim. Phys. Phys.-Chim. Biol.* **1996**, *93*, 1714.
(82) Omta, A. W.; Kropman, M. F.; Woutersen, S.; Bakker, H. J. *Science* **2003**, *301*, 301.
(83) Agmon, N. *J. Mol. Liq.* **2000**, *85*, 87.
(84) Ando, K.; Hynes, J. T. *J. Mol. Liq.* **1995**, *64*, 25.
(85) Ando, K.; Hynes, J. T. *J. Phys. Chem. B* **1997**, *101*, 10464.
(86) Huppert, D.; Kolodney, E.; Gutman, M.; Nachliel, E. *J. Am. Chem. Soc.* **1982**, *104*, 6949.
(87) Lee, J.; Robinson, G. W.; Webb, S. P.; Philips, L. A.; Clark, J. H. *J. Am. Chem. Soc.* **1986**, *108*, 6538.
(88) Robinson, G. W.; Thistlethwaite, P. J.; Lee, J. *J. Phys. Chem.* **1986**, *90*, 4224.
(89) Agmon, N.; Huppert, D.; Masad, A.; Pines, E. *J. Phys. Chem.* **1991**, *95*, 10407. Erratum. *J. Phys. Chem.* **1992**, *96*, 2020.
(90) Cohen, B.; Leiderman, P.; Huppert, D. *J. Phys. Chem. A* **2002**, *106*, 11115.
(91) Green, S.; Xiang, T.; Johnston, K. P.; Fox, M. A. *J. Phys. Chem.* **1995**, *99*, 13787.
(92) Poles, E.; Cohen, B.; Huppert, D. *Isr. J. Chem.* **1999**, *39*, 347.
(93) Cohen, B.; Huppert, D. *J. Phys. Chem. A* **2000**, *104*, 2663.
(94) Melander, L. *Isotope Effects on Reaction Rates*; Ronald Press: New York 1960.
(95) Westheimer, F. H. *Chem. Rev.* **1961**, *61*, 265.
(96) Agmon, N. *Isr. J. Chem.* **1985**, *26*, 375.
(97) Kuznetsov, A. M.; Ulstrup, J. *Can. J. Chem.* **1999**, *77*, 1085.
(98) Robinson, R. A.; Stokes, R. H. *Electrolyte Solutions*, 2nd ed.; Butterworth: London, 1959.
(99) Luz, Z.; Meiboom, S. *J. Am. Chem. Soc.* **1964**, *86*, 4768.
(100) de Grotthuss, C. J. T. *Ann. Chim.* **1806**, *LVIII*, 54.
(101) Danneel, H. *Z. Elektrochem.* **1905**, *11*, 249.
(102) The original paper by von Grotthuss[100] actually deals with hydrogen atom diffusion following the electrolysis of water. The existence of protons was not evident roughly until the beginning of the 20th century,[101] when the work of Grotthuss was recalled and applied to proton mobility.
(103) Bernal, J. D.; Fowler, R. H. *J. Chem. Phys.* **1933**, *1*, 515.
(104) Eigen, M.; De Maeyer, L. *Proc. R. Soc. London A* **1958**, *247*, 505.
(105) Eigen, M. *Ang. Chem., Int. Ed.* **1964**, *3*, 1.
(106) Atkins, P. W. *Physical Chemistry*, 2nd ed.; Oxford University: Oxford, 1982.
(107) Agmon, N. *Isr. J. Chem.* **1999**, *39*, 493.
(108) Walrafen, G. E.; Fisher, M. R.; Hokmabadi, M. S.; Yang, W.-H. *J. Chem. Phys.* **1986**, *85*, 6970.
(109) Onsager, L. In *Physics and Chemistry of Ice*; Whalley, E., Jones, S. J., Gold, L. W., Ed.; Royal Society of Canada: Ottawa, 1973; p 10.
(110) Kunst, M.; Warman, J. M. *J. Phys. Chem.* **1983**, *87*, 4093.
(111) In this estimate we have neglected the self-diffusion of water, $D_{H_2O} = 2.3 \times 10^{-5}$ cm^2/s. Because of the strong HBs in the first solvation shell of H_3O^+, we estimate[81] that the non-Grotthuss contribution to proton mobility (by ordinary diffusion of the oxygen center of H_3O^+) is much smaller than previously suggested.
(112) Zundel, G. In *The Hydrogen Bond, Recent Developments in Theory and Experiments*; Schuster, P., Zundel, G., Sandorfy, C., Eds.; North-Holland: Amsterdam, 1976; pp 687−766.
(113) Zundel, G. *Adv. Chem. Phys.* **2000**, *111*, 1.
(114) Although the H_3O^+ and $H_5O_2^+$ cations have been discussed earlier, they are sometimes dubbed as the "Eigen" and "Zundel" cations, respectively.
(115) Tuckerman, M.; Laasonen, K.; Sprik, M.; Parrinello, M. *J. Phys. Chem.* **1995**, *99*, 5749.
(116) Vuilleumier, R.; Borgis, D. *Isr. J. Chem.* **1999**, *39*, 457.
(117) Kornyshev, A. A.; Kuznetsov, A. M.; Spohr, E.; Ulstrup, J. *J. Phys. Chem. B* **2003**, *107*, 3351.
(118) Sometimes called the "Moses mechanism",[116] due to the analogy with Moses crossing the Red Sea.[80]
(119) Marx, D.; Tuckerman, M. E.; Hutter, J.; Parrinello, M. *Nature* **1999**, *397*, 601.
(120) Atkins, P. W. *Physical Chemistry*, 6th ed.; W. H. Freeman: New York, 1998.
(121) Kobayashi, C.; Saito, S.; Ohmine, I. *J. Chem. Phys.* **2000**, *113*, 9090.
(122) Schmitt, U. W.; Voth, G. A. *J. Phys. Chem. B* **1998**, *102*, 5547.
(123) Day, T. J. F.; Schmitt, U. W.; Voth, G. A. *J. Am. Chem. Soc.* **2000**, *122*, 12027.
(124) Day, T. J. F.; Soudackov, A. V.; Čuma, M.; Schmitt, U. W.; Voth, G. A. *J. Chem. Phys.* **2002**, *117*, 5839.
(125) Zahn, D.; Brickmann, J. *Isr. J. Chem.* **1999**, *39*, 469.
(126) Lapid, H.; Agmon, N.; Petersen, M. K.; Voth, G. A. *J. Chem. Phys.* **2005**, *122*, 014506.
(127) Laws, W. R.; Brand, L. *J. Phys. Chem.* **1979**, *83*, 795.
(128) Harris, C. M.; Selinger, B. K. *J. Phys. Chem.* **1980**, *84*, 1366.
(129) Pines, E.; Huppert, D. *J. Chem. Phys.* **1986**, *84*, 3576.
(130) Agmon, N. *J. Chem. Phys.* **1984**, *81*, 2811.
(131) Pines, E.; Huppert, D.; Agmon, N. *J. Chem. Phys.* **1988**, *88*, 5620.
(132) Agmon, N.; Pines, E.; Huppert, D. *J. Chem. Phys.* **1988**, *88*, 5631.
(133) Gopich, I. V.; Solntsev, K. M.; Agmon, N. *J. Chem. Phys.* **1999**, *110*, 2164.
(134) Agmon, N. *J. Chem. Phys.* **1999**, *110*, 2175.
(135) Gopich, I. V.; Agmon, N. *J. Chem. Phys.* **1999**, *110*, 10433.
(136) Agmon, N.; Hopfield, J. J. *J. Chem. Phys.* **1983**, *78*, 6947. Erratum. *J. Chem. Phys.* **1984**, *80*, 592.
(137) Kosloff, R.; Tal-Ezer, H. *Chem. Phys. Lett.* **1986**, *127*, 223.
(138) Agmon, N.; Kosloff, R. *J. Phys. Chem.* **1987**, *91*, 1988.
(139) Krissinel', E. B.; Agmon, N. *J. Comput. Chem.* **1996**, *17*, 1085.
(140) Kim, H.; Shin, K.-J. *Phys. Rev. Lett.* **1999**, *82*, 1578.
(141) Agmon, N.; Gopich, I. V. *Chem. Phys. Lett.* **1999**, *302*, 399.
(142) Solntsev, K. M.; Huppert, D.; Agmon, N. *Phys. Rev. Lett.* **2001**, *86*, 3427.
(143) Agmon, N.; Szabo, A. *J. Chem. Phys.* **1990**, *92*, 5270.
(144) Pines, E.; Fleming, G. R. *Chem. Phys.* **1994**, *183*, 393.
(145) Solntsev, K. M.; Agmon, N. *Chem. Phys. Lett.* **2000**, *320*, 262.
(146) Ottolenghi, M. *J. Am. Chem. Soc.* **1963**, *85*, 3557.
(147) Pino, G.; Grégoire, G.; Dedonder-Lardeux, C.; Jouvet, C.; Martrenchard, S.; Solgadi, D. *Phys. Chem. Chem. Phys.* **2000**, *2*, 893.
(148) Sobolewski, A. L.; Domcke, W.; Dedonder-Lardeux, C.; Jouvet, C. *Phys. Chem. Chem. Phys.* **2002**, *4*, 1093.
(149) Lee, J.; Robinson, G. W. *J. Am. Chem. Soc.* **1985**, *107*, 6153.
(150) Kuo, J.-L.; Ciobanu, C. V.; Ojamaë, L.; Shavitt, I.; Singer, S. J. *J. Chem. Phys.* **2003**, *118*, 3583.
(151) Agmon, N.; Goldberg, S. Y.; Huppert, D. *J. Mol. Liq.* **1995**, *64*, 161.
(152) Weller, A. *Z. Elektrochem.* **1954**, *58*, 849.
(153) Goldberg, S. Y.; Pines, E.; Huppert, D. *Chem. Phys. Lett.* **1992**, *192*, 77.
(154) Genosar, L.; Cohen, B.; Huppert, D. *J. Phys. Chem. A* **2000**, *104*, 6689.
(155) Cohen, B.; Huppert, D.; Agmon, N. *J. Am. Chem. Soc.* **2000**, *122*, 9838.
(156) Cohen, B.; Huppert, D.; Agmon, N. *J. Phys. Chem. A* **2001**, *105*, 7165.
(157) Cohen, B.; Leiderman, P.; Huppert, D. *J. Lumin.* **2003**, *102*−*103*, 682.
(158) von Smoluchowski, M. *Z. Phys. Chem.* **1917**, *92*, 129.
(159) Tachiya, M. *Rad. Phys. Chem.* **1983**, *21*, 167.
(160) Szabo, A. *J. Phys. Chem.* **1989**, *93*, 6929.
(161) Szabo, A.; Zwanzig, R.; Agmon, N. *Phys. Rev. Lett.* **1988**, *61*, 2496.
(162) Gösele, U. M. *Prog. React. Kinet.* **1984**, *13*, 63.
(163) Nemzek, T. L.; Ware, W. R. *J. Chem. Phys.* **1975**, *62*, 477.
(164) Eads, D. D.; Dismer, B. G.; Fleming, G. R. *J. Chem. Phys.* **1990**, *93*, 1136.
(165) Sikorski, M.; Krystkowiak, E.; Steer, R. P. *J. Photochem. Photobiol. A* **1998**, *117*, 1.
(166) Harris, C. M.; Selinger, B. K. *J. Phys. Chem.* **1980**, *84*, 891.

(167) Weller, A. *Z. Phys. Chem. NF* **1958**, *15*, 438.
(168) Huppert, D.; Goldberg, S. Y.; Masad, A.; Agmon, N. *Phys. Rev. Lett.* **1992**, *68*, 3932.
(169) Solntsev, K. M.; Huppert, D.; Agmon, N. *J. Phys. Chem. A* **2001**, *105*, 5868.
(170) Pines, D.; Pines, E. *J. Chem. Phys.* **2001**, *115*, 951.
(171) Edelstein, A. L.; Agmon, N. *J. Phys. Chem.* **1995**, *99*, 5389.
(172) Kim, H.; Yang, M.; Shin, K. J. *J. Chem. Phys.* **1999**, *111*, 1068.
(173) Popov, A. V.; Agmon, N. *J. Chem. Phys.* **2001**, *115*, 8921.
(174) Popov, A. V.; Agmon, N. *J. Chem. Phys.* **2002**, *117*, 4376.
(175) Sung, J.; Lee, S. *J. Chem. Phys.* **1999**, *111*, 796.
(176) Naumann, W.; Shokhirev, N. V.; Szabo, A. *Phys. Rev. Lett.* **1997**, *79*, 3074.
(177) Sung, J.; Shin, K. J.; Lee, S. *J. Chem. Phys.* **1997**, *107*, 9418.
(178) Gopich, I. V.; Agmon, N. *Phys. Rev. Lett.* **2000**, *84*, 2730.
(179) Agmon, N.; Gopich, I. V. *J. Chem. Phys.* **2000**, *112*, 2863.
(180) Oh, C.; Kim, H.; Shin, K. J. *J. Chem. Phys.* **2002**, *117*, 3269.
(181) Popov, A. V.; Agmon, N.; Gopich, I. V.; Szabo, A. *J. Chem. Phys.* **2004**, *120*, 6111.
(182) Förster, T.; Völker, S. *Chem. Phys. Lett.* **1975**, *34*, 1.
(183) Hauser, M.; Haar, H.-P.; Klein, U. K. A. *Ber. Bunsen-Ges. Phys. Chem.* **1977**, *81*, 27.
(184) Agmon, N. *J. Chem. Phys.* **1988**, *89*, 1524.
(185) Bardez, E.; Devol, I.; Larrey, B.; Valeur, B. *J. Phys. Chem. B* **1997**, *101*, 7786.
(186) Bardez, E.; Alain, V.; Destandau, E.; Fedorov, A.; Martinho, J. M. G. *J. Phys. Chem. A* **2001**, *105*, 10613.
(187) Bardez, E.; Goguillon, B.-T.; Keh, E.; Valeur, B. *J. Phys. Chem.* **1984**, *88*, 1909.
(188) Il'ichev, Y. V.; Demyashkevich, A. B.; Kuzmin, M. G. *J. Phys. Chem.* **1991**, *95*, 3438.
(189) Cohen, B.; Huppert, D.; Solntsev, K. M.; Tsfadia, Y.; Nachliel, E.; Gutman, M. *J. Am. Chem. Soc.* **2002**, *124*, 7539.
(190) Bhattacharyya, K. *Acc. Chem. Res.* **2003**, *36*, 95.
(191) Gutman, M.; Nachliel, E. *Annu. Rev. Phys. Chem.* **1997**, *48*, 329.
(192) Bransburg-Zabary, S.; Nachliel, E.; Gutman, M. *Biophys. J.* **2002**, *83*, 2987.
(193) Chattoraj, M.; King, B. A.; Bublitz, G. U.; Boxer, S. G. *Proc. Natl. Acad. Sci., U.S.A.* **1996**, *93*, 8362.
(194) Lossau, H.; Kummer, A.; Heinecke, R.; Pöllinger-Dammer, F.; Kompa, C.; Bieser, G.; Jonsson, T.; Silva, C. M.; Yang, M. M.; Youvan, D. C.; Michel-Beyerle, M. *Chem. Phys.* **1996**, *213*, l.